



UNIVERSITY OF CAMBRIDGE

Investigating the role of CSA in nuclear envelope integrity maintenance

CANDIDATE: *Austin Lai*

Churchill College



SUPERVISION BY

Dr Delphine Larrieu

IN PARTIAL FULFILLMENT OF THE REQUIREMENTS

FOR THE DEGREE OF

MASTER OF PHILOSOPHY

IN THE SUBJECT OF

MEDICAL SCIENCE

August 2021

Declaration: This thesis is the result of my own work and includes nothing which is the outcome of work done in collaboration except where specifically indicated in the text.

Statement of Length: This dissertation does not exceed the word limit of 20,000 words.

The word count excluding figure legends, tables, and references: 6,489

Total Word Count: 11,737

ACKNOWLEDGEMENTS

This report is a product of nine months of research conducted in Dr Delphine Larrieu's laboratory. During this time, I worked under the guidance of Dr Delphine Larrieu and Dr Anne Janssen, a postdoctoral fellow in the lab. I developed my understanding of and technical skills in tissue culture management, biochemical techniques, and microscopy. I gained further experience in designing experiments and forming hypotheses based on previous data. Additionally, I had the opportunity to present parts of my findings at the annual retreat for the Cambridge Institute for Medical Research (CIMR), as well as the biweekly Cell Biology Seminar.

A single-year project under the unusual circumstances of the COVID pandemic posed numerous additional challenges. However, the support and guidance provided by Dr Larrieu and Dr Janssen cannot be overstated. From the daily update meeting through video conference calls to the additional time taken by both to teach me ways to improve the biochemical experiments, much of what I have learned this year would not have been possible without their patience and mentorship. The supportive environment established by other members of the lab, including Dr Sophia Breusegem, Jonathan Lam, and Romain Bucci were also crucial and highly appreciated.

I would like to thank Matthew Gratian of the CIMR microscopy facility for providing excellent training on the confocal microscope, and the Flow Cytometry facility to assisting with the sorting of various cell lines throughout the project.

At the time of this thesis' submission, I worked in the Larrieu Lab between 2nd October 2020 to 15th August 2021. I participated in weekly lab meetings, in which I provided an update on my progress and discussed my results with colleagues in the lab. I also participated in fortnightly journal clubs, which lasted until June, during which we discussed recent publications in the field.

ABSTRACT

Introduction: Cockayne syndrome (CS) is a premature ageing disorder characterised by a wide range of debilitating symptoms. The average lifespan of CS patients is fourteen years, with no available treatment or cure. CS can result from numerous mutations in *ERCC8* or *ERCC6*, encoding Cockayne Syndrome A (CSA) or B (CSB) proteins, respectively. Proteins CSA and CSB are classically known to play roles in repairing UV-induced DNA damage by mediating transcription-coupled nucleotide excision repair (TC-NER). Recently, our lab observed abnormal nuclear morphology in CSA patient cell lines as well as in cells depleted for CSA – but not CSB. Abnormal nuclear shape is also a characteristic of other premature ageing syndromes, in which misshapen nuclei are caused by drastic changes in nuclear envelope (NE) integrity, contributing to the ageing phenotypes. However, the potential role of CSA in maintaining nuclear envelope integrity had never been reported. We hypothesised that CSA might play a new, noncanonical role in maintaining nuclear envelope integrity.

Methods: To investigate the effects of the loss of CSA on the nuclear envelope integrity, we used an immortalised CSA patient-derived cell line (CS-A), carrying a loss-of-function missense mutation in *ERCC8*, together with the isogenic cell line stably expressing hemagglutinin-tagged CSA (HA-CSA) (termed WT). We used western blotting to study the level of various proteins, including the cytosolic DNA sensing cGAS-STING pathway and nuclear envelope proteins. We also analysed the nuclear envelope integrity of CSA and CSB patient-derived fibroblasts by immunofluorescence microscopy. Using the software CellProfiler™, we analysed the nuclear shape, nuclear blebs, and subcellular localisation of different proteins.

Results: We confirmed that the loss of CSA in patient-derived (CS-A) fibroblasts results in increased nuclear deformation, nuclear envelope rupture, and micronuclei formation. Further, the loss of CSA increased the activity of the cGAS-STING innate immune signalling pathway. Unexpectedly, we observed in CS-A fibroblasts a proteasome-dependent reduction of barrier-to-autointegration factor (BAF), an abundant DNA-binding and NE protein with an emerging role in nuclear envelope rupture repair. Overexpression of BAF reduced the nuclear envelope ruptures in the CS-A cells. Finally, the role of CSA in the maintenance of nuclear envelope integrity appears to be independent of its function in UV-induced DNA damage repair.

Discussion: Our results suggest that CSA is necessary for the maintenance of nuclear envelope integrity. Furthermore, the upregulation of the cGAS-STING pathway that we observed in CSA patient-derived cells appears to be caused by nuclear envelope ruptures. As this pathway is known to be involved in inflammation and ageing, our data suggest that the nuclear envelope ruptures occurring in the absence of CSA may underlie some aspects of Cockayne Syndrome A and contribute to some of the patients' phenotypes.

TABLE OF CONTENTS

Introduction	6
Premature ageing syndromes	6
Clinical presentation of Cockayne syndrome (CS)	6
Genetic aetiology of CS, and the functions of CSA and CSB	8
The nuclear envelope (NE)	11
Materials and Methods	17
Results	35
Loss of CSA results in aberrant nuclear morphology.	35
Loss of CSA decreases intensity of DAPI signal.	36
Loss of CSA increases the formation of nuclear blebs and micronuclei.	37
Loss of CSA results in NE ruptures and activation of the cGAS/STING pathway.	38
CSA does not interact with core NE proteins and does not modulate their levels or localisation.	40
Loss of CSA results in decreased barrier-to-autointegration factor (BAF) levels.	41
BAF is reduced in a proteasome-dependent manner in CS-A cells.	43
Overexpression of BAF reduces NE ruptures.	44
The NE function of CSA is independent of its canonical function in DNA damage repair.	47
Conclusion	49
Discussion	49
References	53

INTRODUCTION

Premature ageing syndromes

Premature ageing syndromes, also known as progeroid disorders, represent a collection of diseases that share a wide range of clinical manifestations, including loss of vision and hearing, atrophy, progressive neurodegeneration, cardiovascular defects, and osteoporosis (Rieckher et al., 2021). Progeroid disorders can be classified into two subtypes: those that are caused by nuclear envelope instability and those that are due to impaired DNA-damage response (DDR) or DNA repair (Carrero et al., 2016; Rieckher et al., 2021). The former includes Hutchinson-Gilford progeria syndrome (HGPS), Néstor-Guillermo progeria syndrome (NGPS), restrictive dermopathy (RD), atypical progeria syndromes (APSs), and mandibuloacral dysplasia (MAD) (Carrero et al., 2016). The latter includes Ataxia-telangiectasia (A-T), Bloom syndrome, Fanconi anaemia (FA), Werner syndrome (WS), xeroderma pigmentosum (XP), and Cockayne syndrome (CS) (Carrero et al., 2016). The phenotypes observed in normal ageing are recapitulated to various extents in premature ageing disorders (Carrero et al., 2016). These overlaps in clinical and molecular phenotypes suggest that a further understanding of progeroid disorders may provide insights into the normal process of ageing. The work presented in this thesis will be focusing on Cockayne syndrome.

Clinical presentation of Cockayne syndrome (CS)

First identified in 1936 by Edward Cockayne (Cockayne, 1936), Cockayne syndrome (CS) is an autosomal recessive disorder affecting multiple organ systems (Laugel, 2013). CS patients generally present a wide range of symptoms including growth failure, intellectual disability, neurodegeneration, limb hypertonia and spasticity, cerebellar ataxia, tremor, and dysarthric speech (**Figure 1**) (Laugel, 2013; Wilson et al., 2016). Data in the United States estimates that CS affects approximately 1 in 250,000 live births (<https://rarediseases.org/rare-diseases/cockayne-syndrome/>). CS patients consistently demonstrate similar phenotypes with different time of onset (Laugel, 2013). Clinical studies refined and subdivided CS into three types based on the time of onset. In addition to the classical (Type I) CS, early-onset cases (Lowry, 1982; Moyer et al., 1982) became known as type II, while Type III CS is late-onset (Kennedy et al., 1980; Rapin et al., 2006). These different CS subtypes do not seem to differ consistently in their severity or symptoms. Several other diseases share phenotypes and genetic aetiology with CS.

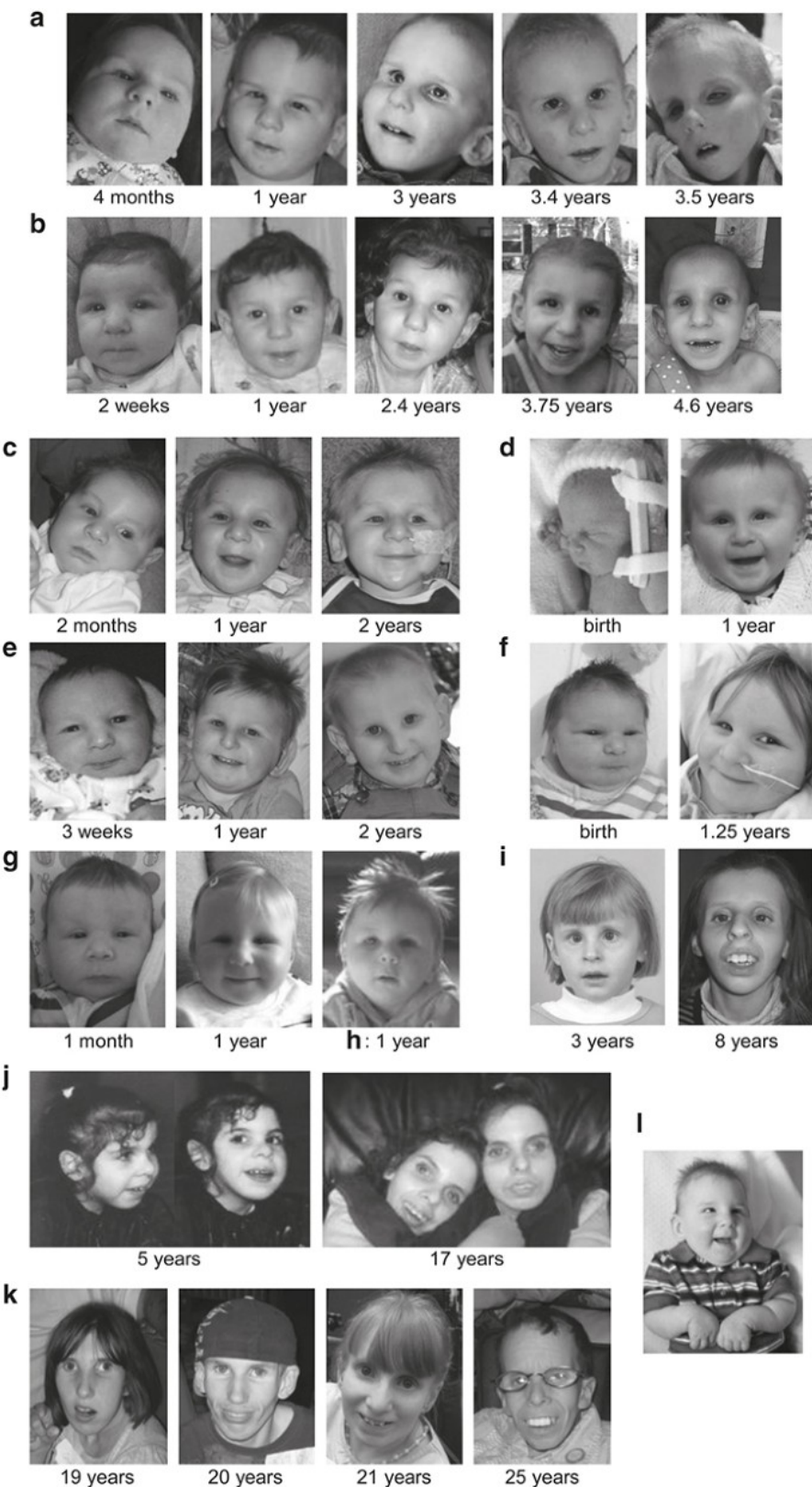


Figure 1. (A-I) Study participants from the Cockayne Syndrome Natural History (CoSyNH) study (Wilson et al., 2016). Patients shown in (g, h) are sister and brother. (j) Identical twins shown at age 5 and 17. (k) Aggregate images of older patients with CS. (l) Patient demonstrates flexed upper limb posture occasionally observed in patients with CS. Figure taken from (Wilson et al., 2016).

Cerebro-oculo-facio-skeletal syndrome (COFS) includes severe symptoms that develops due to an extremely early onset of CS. UV-sensitive syndrome (UVSS) is a much milder disease, involving cutaneous photosensitivity. In terms of severity, CS spans from most to least severe: COFS, CS Type II (early-onset), CS Type I (classical), CS Type III (late-onset), UVSS.

Genetic aetiology of CS, and the functions of CSA and CSB

In the 1990s, the developments in genetic testing allowed for the identification of the two genes responsible for CS: *ERCC6* (Excision Repair 6, Chromatin Remodelling Factor) encoding for CSB and *ERCC8* encoding for CSA. Both CSB and CSA are important factors in the transcription-coupled nucleotide excision repair (TC-NER), a crucial process that removes DNA lesions such as 6-4 pyrimidine-pyrimidone photoproducts (6-4 PPs) and cyclobutane-pyrimidine dimers (CPDs) that can be induced by UV irradiation (Marteijn et al., 2014). By blocking RNA polymerase (RNA Pol) II, these unresolved DNA damages can arrest transcription and trigger cell death (Ljungman and Zhang, 1996). Defects in TC-NER therefore underlie the UV sensitivity characteristic of CS patient-derived fibroblasts. The TC-NER pathway indirectly detects DNA lesions through the stalling of RNA Pol II (**Figure 2A**) and serves to translocate the polymerase backwards from the mutation site or remove it from the transcription site altogether (Svejstrup, 2002). In the absence of UV irradiation, CSB interacts with RNA Pol II to promote transcription elongation (Sarker et al., 2005; Tantin et al., 1997). Upon UV irradiation, the CSB-RNA Pol II binding is stabilised (van den Boom et al., 2004) (**Figure 2B**). In addition to interacting with RNA Pol II, CSB is part of the SNF/SWI2 subfamily of chromatin remodelling ATPases (Citterio et al., 2000). As a chromatin remodelling factor, CSB loosens the nucleosome structure around the stalled polymerase (**Figure 2B**) (Citterio et al., 2000). Furthermore, the CSB-RNA Pol II binding leads to the recruitment of the CSA complex, the UVSSA complex, and core NER factors (Fousteri et al., 2006; Saijo, 2013) (**Figure 2C**). The CSA complex, including the Damage-specific DNA binding protein 1 (DDB1), Cullin-4A (CUL4A), and regulator of cullins-1 (Roc1), functions as an

E3 ubiquitin ligase that is responsible for the UV-dependent ubiquitination of CSB (Fousteri et al., 2006; Groisman et al., 2003; Saijo, 2013). E3 ubiquitin ligases act as the third and final member of a series of ubiquitin ligases that covalently conjugate the peptide ubiquitin onto target proteins. Proteins conjugated with a poly-ubiquitin chain can be targeted for protein degradation (Doherty et al., 2002). This degradation occurs through the 26S proteasome, which is present in both the cytosol and the nucleus (Doherty et al., 2002). CSA is not found to interact directly with RNA Pol II *in vivo* (Fousteri et al., 2006). The UVSSA complex, on the other hand, antagonises ubiquitination by the CSA complex at the NER site. Both CSA and UVSSA complexes are necessary for the proper regulation of TC-NER, and for removal of DNA lesions (Fousteri and Mullenders, 2008).

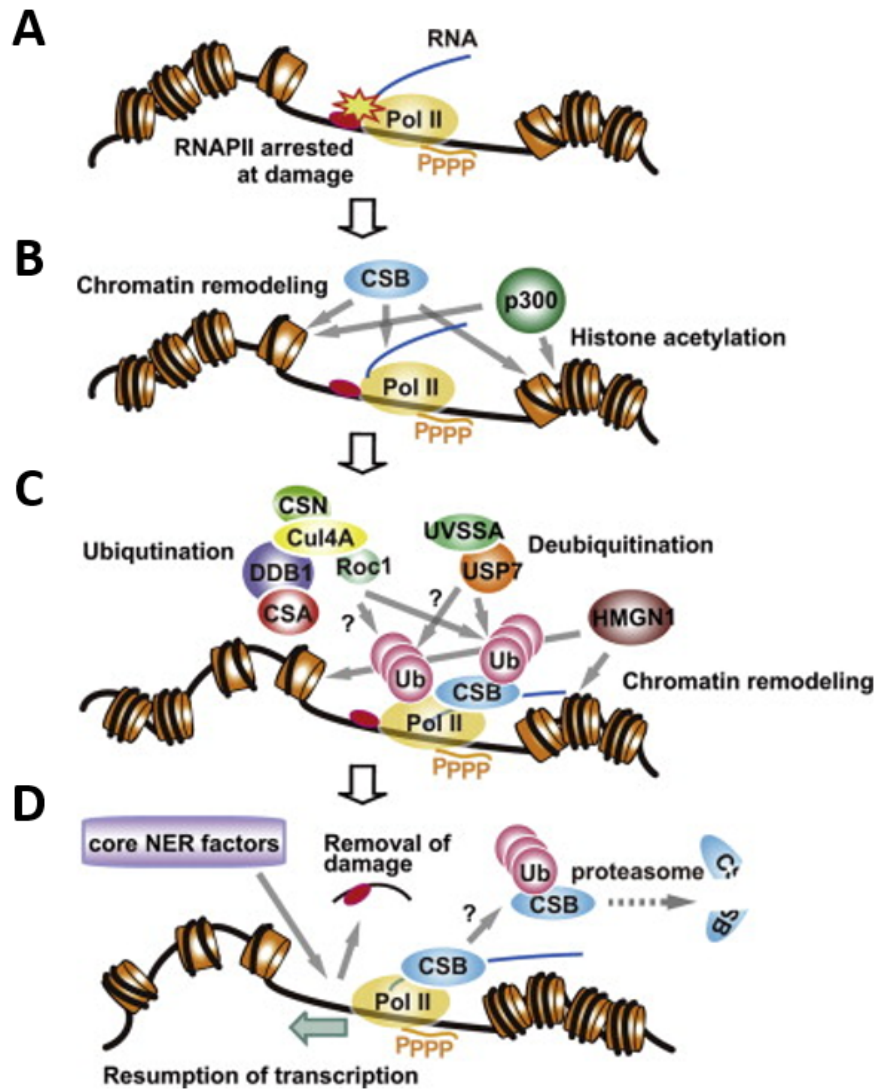


Figure 2. A model for the roles of CSA and CSB in TC-NER. (A) During transcription, RNA Pol II encounters a lesion and becomes stalled. (B) At this point, CSB is recruited to the stalled RNA Pol II. (C) CSA, in complex with Cul4A, DDB1, and Roc1, and UVSSA, in complex with USP7 are recruited to the stalled Pol II-CSB. The CSA complex functions as ubiquitin ligase. The UVSSA complex functions as a deubiquitinase. The regulated ubiquitination around the stalled RNA Pol II site has implications for the mechanism of TC-NER. CSB, p300, and HMGN1 function as chromatin remodelling factors around the stalled RNA Pol II site. (D) The regulation of ubiquitination by the CSA and UVSSA complexes facilitates the progression of TC-NER to remove the DNA lesion. Figure adapted from (Saijo, 2013).

CSB belongs to the large family of helicases called helicase superfamily 2 (SF2) (Lake and Fan, 2013) and can modify DNA conformation. CSB contains three major domains: a central ATPase domain flanked by an N-terminal region and a C-terminal region (Lake and Fan, 2013). Regions flanking the central ATPase domain determine CSB protein autoregulation and localisation, with the presence of nuclear localisation sequence (NLS) in each region. CSB may harbour missense mutations in its catalytic core, some of which may prevent DNA from being able to stimulate ATPase activity of CSB or reduce ATP hydrolysis efficiency (Laugel, 2013). Cockayne syndrome B may also result from small deletion mutations in the catalytic regions, disrupting ATP hydrolysis. Missense mutations in non-catalytic regions are in C-terminal NLS but do not disrupt nuclear localisation of CSB due to the additional NLS in the other side of the ATPase domain (Lake et al., 2010), but is disease associated. Interestingly, there is no known disease-associated missense mutations in N-term, suggesting that N-term is perhaps not as important for CSB function.

The seven WD40 repeat motifs in CSA are crucial for its interaction with other protein partners (Laugel, 2013). CSA is required for the recruitment of UVSSA to stalled RNA polymerase II. CSA patients can harbour missense, deletion, nonsense, and frame shift mutations in CSA. All eight recorded missense mutations are in the WD40 domain (**Figure 3**), impeding the ability of CSA to associate with other proteins (Jin et al., 2006; Saijo, 2013). All nonsense and deletion mutations in CSA result in the loss of at least one WD40 motifs, thus abolishing CSA function (Saijo, 2013).

CSA / ERCC8

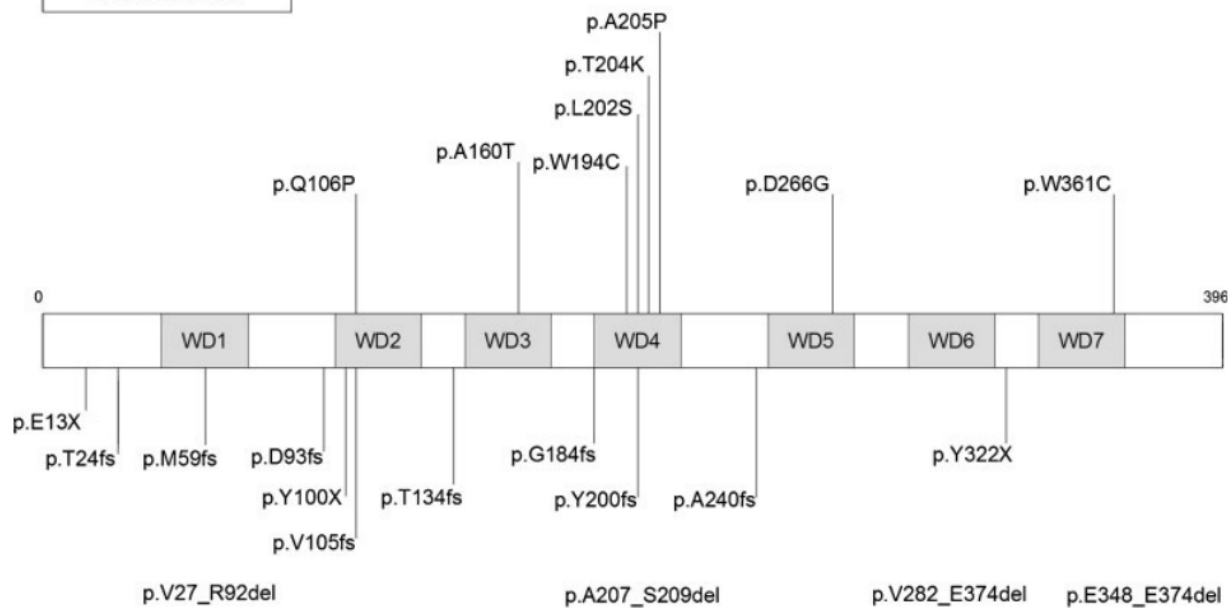


Figure 3. Mutation map of the ERCC8 (CSA) gene. Missense mutations are annotated above the protein sequence, while other point mutations and deletions are shown beneath the sequence. WD domains are highlighted in grey. Figure adapted from (Laugel et al., 2010).

In the work presented here, we used patient cell lines from Cockayne Syndrome, and identified a new function for CSA in regulating the nuclear envelope integrity, which is independent of its known functions described above. I will therefore now introduce a few concepts related to the nuclear envelope.

The nuclear envelope (NE)

Key structural components of the NE

The nuclear envelope is made up of two lipid bilayers—the outer nuclear membrane (ONM) and the inner nuclear membrane (INM) (**Figure 4**). The ONM is contiguous with the endoplasmic reticulum (ER), and the two bilayers fuse at the nuclear pore complexes (NPC), a protein complex that allows import and export across the NE in a highly regulated manner (Hetzer, 2010; Maciejowski and Hatch, 2020).

Closely interacting and supporting the INM is the nuclear lamina. The nuclear lamina is a thin meshwork, approximately 40 to 100 nm in thickness, comprised mainly of nuclear lamins.

There are two structurally distinct types of lamins: A-type lamins, which include lamin A and its splice variant C, and B-type lamins, which include lamins B1 and B2. To date, 30 diseases have been associated with mutations in the *LMNA* gene or related NE genes (Wong and Stewart, 2020). These diseases, also known as laminopathies, affect a wide range of organ systems. For example, Emery-Dreifuss muscular dystrophy (EDMD), the first discovered laminopathy, is caused by mutations in lamin A/C or Emerin (Bione et al., 1994; Bonne et al., 1999). These components of the nuclear envelope altogether maintain the structural integrity and shape of the nucleus. The shape of the nucleus varies from cell type to cell type. For example, the nuclei of fibroblasts usually exhibit ovoidal and more or less elongated shape, while immune cells that specialise in infiltrating physiological structures often take on irregular shape (Srivastava et al., 2021). Nuclear shape also varies depending on the stage of cell cycle. Transitioning from G1 to S/G2 phases, the natural fluctuation of the non-dividing nucleus stabilises and tension increases (Chu et al., 2017).

The nuclear envelope also forms contacts with the chromatin through chromatin-lamina interactions, which are facilitated by NE protein such as LEM-domain proteins like emerin, as well as barrier-to-autointegration factor 1 (BAF) (Srivastava et al., 2021). Mutation in these proteins can destabilise the nuclear integrity (Funkhouser et al., 2013). As the heterochromatin is anchored to the NE, disruption of the NE-chromatin interactions through mutations or mechanical stress can result in deregulation of transcription (Van de Vosse et al., 2011).

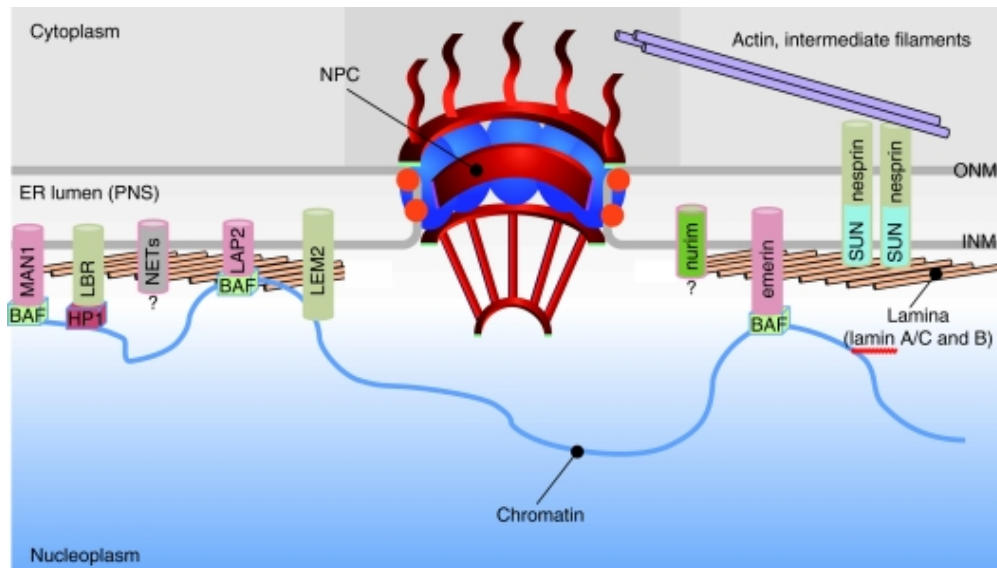


Figure 4. Main structural components of the nuclear envelope. The nuclear membrane is fundamentally composed of the ONM and INM, and the perinuclear space in between. Through

NE transmembrane proteins such as SUN1 and nesprin proteins, the nuclear envelope is connected to the cytoskeleton, allowing it to sense and respond to mechanical compressions. The Lamin B receptor (LBR), shown in dark green, with both B-type lamins and other chromatin-associated proteins (e.g., HP1 γ). LEM-domain family proteins, shown in pink, bind to lamins and interact with chromatin through barrier-to-autointegration factor (BAF). Figure adapted from (Hetzer, 2010).

NE rupture and NE rupture repair

The loss of nuclear lamina, either by mutation in lamin proteins (Earle et al., 2020; Goldman et al., 2004; Muchir et al., 2004) or knockdown of lamin A/C (Raab et al., 2016) can lead to nuclear envelope ruptures during interphase. To summarise, the formation of NE ruptures is often preceded by the deformation of the NE and the formation of nuclear blebs (**Figure 5**). Mechanical stress applied on cells can challenge the NE integrity. When the deformation is severe enough, the NE can lose its attachment to the lamina and chromatin, and form protrusions (Srivastava et al., 2021). These protrusions of the NE are called nuclear blebs (**Figure 5B**). On rare occasions, nuclear blebs can result from the separation of lamin A/C from lamin B (Lionetti et al., 2020) or the lamina from the chromatin (Stephens et al., 2017). The double membrane of the nuclear blebs lacks most NE proteins such as the Linker of Nucleoskeleton and Cytoskeleton (LINC) complex and nuclear pore complex (Srivastava et al., 2021). The formation of nuclear blebs is almost always followed by nuclear envelope rupture leading to the outward herniation of the chromatin which can result in genomic instability (Srivastava et al., 2021) (**Figure 5D**). Then, the rupture is rapidly repaired (Earle et al., 2020; Raab et al., 2016) (**Figure 5E**). In the case of chromatin herniation, the nuclear lamina reforms along the external surface of the chromatin, preceding the full resealing of the nuclear envelope (Charras et al., 2008) (**Figure 5F**).

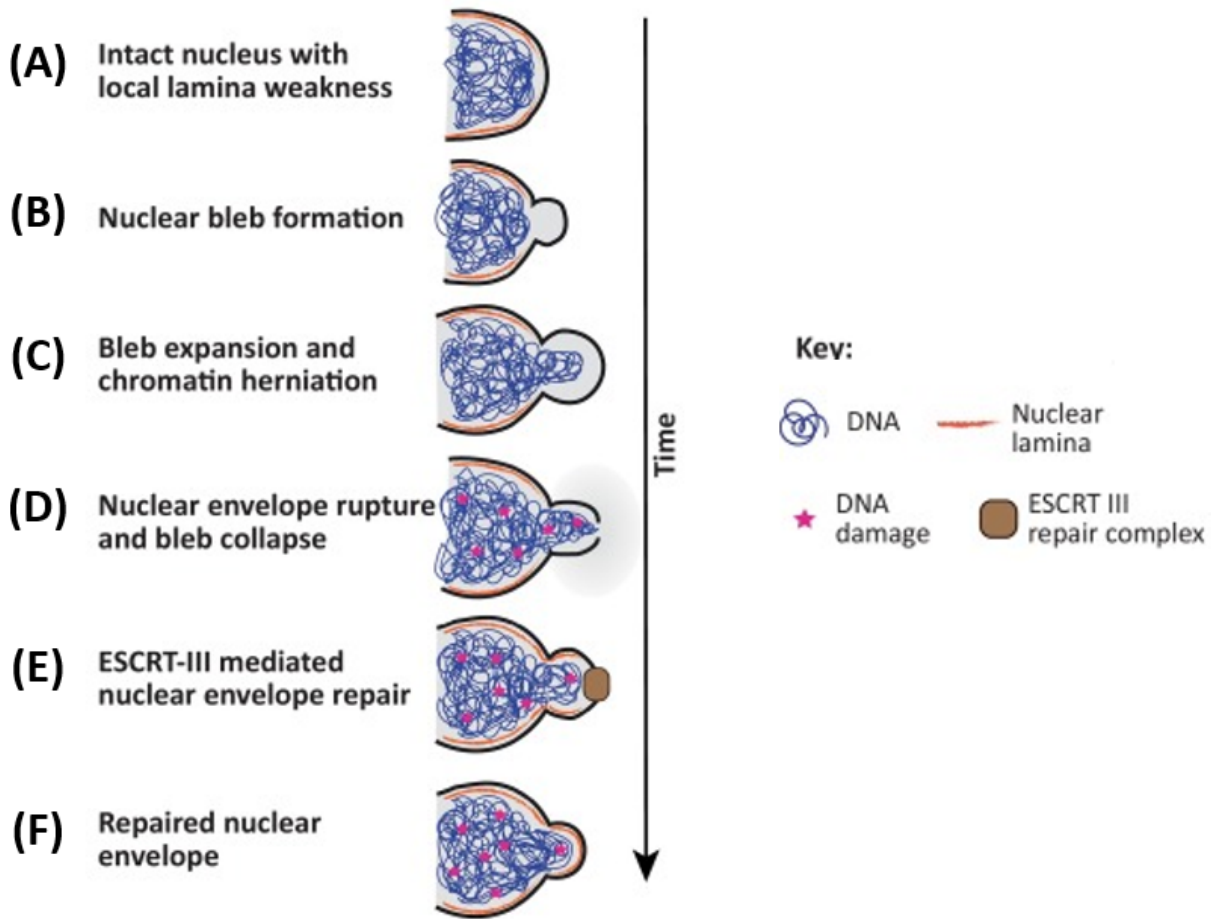


Figure 5. Schematic representation of nuclear bleb formation, nuclear rupture, and rupture repair events. Mechanical force by artificial means such as compression systems or natural cell compression is transmitted to the nucleus through the cytoskeleton. (A) Nucleus prior to compression (B) Compression of the nucleus increases intranuclear pressure, resulting in detachment of the nuclear membranes from the underlying nuclear lamina. Nuclear bleb begins to form at gaps in the lamina (orange lining) and high nuclear curvature. (C) Further compression of the nucleus causes the nuclear membrane bleb to expand. Chromatin can protrude through the lamina gap into the bleb. (D) The nuclear membrane at the bleb subsequently ruptures. This opening leads to uncontrolled exchange between the nuclear and cytoplasmic compartments. Nuclear deformation and NE rupture result in DNA damage (pink stars). (E) Ruptures in the nuclear membrane can be repaired by the ESCRT-III machinery (brown rectangle). (F) DNA damage persists even after the nucleus has passed through the constriction and NE integrity has been restored. Figure adapted from (Shah et al., 2017).

The expression and abundance of NE proteins influences the level of mechanical force required to detach the nuclear membrane (Lee and Burke, 2018). For instance, SUN domain-containing protein 1 (SUN1), anchors the NE to the lamina meshwork, strengthening the NE integrity. Additionally, intermediate filaments such as vimentin can strengthen the nuclear integrity and render the nucleus more resistant against mechanical strain (Stankevicius et al., 2019). Overcoming the resistance provided by these nuclear envelope proteins and intermediate filaments, the nuclear envelope also has large folds which can open upon nuclear deformation (Le Berre et al., 2012; Venturini et al., 2020). Beyond this unfolding, the NE will begin to stretch, ultimately leading to forming blebs and nuclear rupture.

NE ruptures are repaired on the scale of mostly minutes, and occasionally hours. If repaired properly, they don't cause cell death and the long-term effects of these ruptures are still unclear. Several nuclear envelope rupture repair mechanisms have been proposed. Broadly, these are: recruiting ER sheets to the exposed chromatin, spreading the existing ONM, plugging the rupture through membrane recruitment, and resealing by protein complexes (Maciejowski and Hatch, 2020). Here, we focus on the mechanism involving membrane resealing by protein complexes.

Following a rupture at the nuclear membrane, NE assembly proteins that includes lamin A, BAF, LEM-domain proteins, and the endosomal sorting complexes required for transport (ESCRT)-III remodelling complex (Denais et al., 2016; Halfmann et al., 2019; Le Berre et al., 2012; Penfield et al., 2018; Raab et al., 2016) are recruited to the site of rupture. BAF is required for the recruitment of the LEM-domain NE proteins at the rupture (Samwer et al., 2017). The small, 10-kDa protein BAF normally functions as a homodimer to cross-link DNA (Jamin and Wiebe, 2015). It is a crucial component in initiating the reformation of the nuclear envelope after cell division (Samwer et al., 2017). More recent data suggests a requirement for BAF in the recruitment of ESCRT-III to nuclear envelope ruptures, by binding to LEMD2, leading to subsequent interaction between LEMD2 and Charged Multivesicular Body Protein (CHMP7) (Gu et al., 2017; Olmos et al., 2016; von Appen et al., 2020; Webster et al., 2016). Experimental disruption of LEMD2-BAF interaction inhibits ESCRT-III recruitment and cause nuclear morphology defects consistent with delayed membrane sealing (von Appen et al., 2020). While recent work has begun to shed light on the function of BAF in the context of ESCRT-mediated resealing of the membrane, much remains to be clarified. The varying effects of knocking down different NE or ESCRT-III proteins on the duration of membrane rupture suggest a potential context-dependence of ESCRT-

III function. Furthermore, the overactivity of CHMP7 has been shown to induce nuclear membrane ruptures in an ESCRT-III-dependent manner (Vietri et al., 2020b).

Micronucleus (MN) formation and rupture

Another event that involves NE rupture is mitosis. During mitotic cell division, the NE breaks down, the chromosomes segregate, before the NE reforms around the nucleus of each daughter cell (Güttinger et al., 2009; Ungricht and Kutay, 2017). Micronuclei (MN) can arise from lagging chromosomes or chromosome fragments caused by mitotic errors or DNA damage (Cimini et al., 2004; Kwon et al., 2020; Thompson and Compton, 2011). MN have been used as a biomarker for tumour risk (Stich and Rosin, 1984), tumour grade (Thompson and Compton, 2011), and genotoxicity (Evans et al., 1959). As in primary nuclei, the NE of MN is fragile and can rupture through mechanisms similar to those discussed above. When the MN NE ruptures, the DNA within the MN can activate innate immune signalling pathways, such as the cGAS-STING pathway, that can result in proinflammatory response (Bakhoum et al., 2018; Mackenzie et al., 2017). Hyperactivation of inflammatory signalling pathways is a common feature of ageing (López-Otín et al., 2013), cancer (Hanahan and Weinberg, 2011), and autoimmune disorders (Crow and Manel, 2015).

Our knowledge of CS, the functions of CSA and CSB, as well as NE integrity in progeroid diseases led us to consider whether NE abnormalities may play a role in CS. Further, members of our lab previously observed that cells with the loss of CSA, but not CSB, showed abnormal nuclear morphology. These background knowledge and preliminary observation altogether led us to hypothesise that CSA plays a role in maintaining the integrity of the NE, and that the loss of CSA contributes to some phenotypes of CS that cannot be explained by the canonical role of CSA in UV-induced DNA damage repair. This hypothesis led us to address four aims: first, establishing the link between CSA function and the maintenance of NE integrity; second, exploring the downstream consequences of the loss of NE integrity in CS patient-derived cells; third, investigating how specific NE proteins are affected by the loss of CSA; and finally, searching for potential strategies to rescue nuclear defects in CS.

MATERIALS AND METHODS

Cell culture and transfections

CSA patient-derived skin fibroblasts (CS3BE) and CSB patient-derived skin fibroblasts (CS1AN) were purchased from Coriell Cell Repositories and used between passage number 9-26. CS3BE cell line stably expressing HA-CSA (termed WT cells in this report) was a gift from Dr Sebastian Iben (Ulm University, Germany) and is grown in complete media containing 50 µg/mL Geneticin (G418, Life Technologies) to maintain plasmid expression. hTERT immortalised fibroblasts are AG10803 control human fibroblasts that have been immortalised with SV40LT and TERT obtained from the laboratory of Carlos López-Otin at the Department of Biochemistry and Molecular Biology of the Universidad de Oviedo, Spain. Cells were grown in Dulbecco's modified Eagle medium (DMEM, Sigma-Aldrich) supplemented with 10% fetal-bovine serum (FBS, BioSera), 2mM L-glutamine, 100U/ml penicillin and 100ug/ml streptomycin (complete media). Plasmid DNA transfactions were carried out using Lipofectamine-2000 or Trans-IT transfection reagents, following the manufacturer's protocol, and incubated for 24-hours in complete media.

Western Blotting/Immunoprecipitations

Protein extracts were prepared by scraping cells in sodium dodecyl sulfate (SDS) lysis buffer (4% SDS, 20% glycerol, 120mM Tris-HCl, pH 6.8), boiling for 5 minutes at 95°C, followed by 20 strokes through a 25-gauge needle. Prior to loading, lysates were diluted with NuPAGE™ Sample Buffer (ThermoFischer) and 200mM dithiothreitol (dT) and further boiled for 10 minutes. Proteins were then resolved on a 4-12% gradient gel (NUPAGE, Life Sciences) and transferred onto a nitrocellulose membrane (Protran; Whatman). Secondary antibodies conjugated to IRDye 680/790CM were from LI-COR Biosciences. Detection and quantification were performed with an imager (Odyssey; LI-COR Biosciences). Buffers used as well as antibody information can be found below. For Immunoprecipitation (IP), cells were harvested in IP buffer (150mM NaCl, 0.1% Triton, 50mM Tris-HCl pH 8, 1mM EDTA, 1mM DTT) freshly supplemented with EDTA-free protease inhibitor cocktail (Roche). Cell lysis was performed on ice for 10 minutes, with agitation every 5 minutes followed by centrifugation (13000 x g, 15 minutes). Protein concentration was measured by a NanoDrop spectrophotometer (ThermoFischer). 0.25mg Pierce™ Anti-HA magnetic beads were washed 3 times in 1mL of IP buffer and subsequently incubated at 4°C with rotation with lysates for 2 hours. Protein-bound beads were then washed in IP buffer and

resuspended in NuPAGE™ Sample Buffer/dTT, boiled for 10 minute and analysed as per Western blot protocol above.

Immunofluorescence microscopy

Cells were seeded on 12mm plastic coverslips prior to any experimental procedure. Cells were washed with PBS, fixed for 10 minutes with 4% PFA and subsequently permeabilised for 5 minutes with PBS/0.2% Triton X-100, and blocked with PBS/0.2% Tween-20 (PBS-T) containing 5% BSA for 1 hour. Coverslips were then incubated with primary antibody for 1 hour, washed three times with PBS and subsequently incubated for an additional 30 minutes with secondary antibodies coupled to Alexa Fluor 488, 568 or 647 fluorophores (Life Technologies, see Table 6 for antibody information), before being incubated with DAPI (1/5000 dilution). Images were acquired with a Zeiss AxioImager Z2 Upright Wide-field microscope using a 63x oil objective. Analysis was performed using Image-J.

Table 1. Catalogue of reagents and resources.

Reagents/Resource	Dilution/Concentration	Source	Identifier
Antibodies			
Anti-Lamin A/C	1:500 (Immunofluorescence) 1:1000 (Western Blot)	Santa Cruz	sc-7292
Anti-Lamin B	1:500 (Immunofluorescence)	Santa Cruz	sc-365214
Anti-LEMD2	1:200 (Immunofluorescence)	Sigma	HPA017340
Anti-CSA	1:1000 (Western Blot)	Santa Cruz	sc-376981
Anti-cGAS	1:1000 (Western Blot)	Cell Signaling	D1D3G
Anti-pTBK	1:1000 (Western Blot)	Cell Signaling	5483
Anti-TBK	1:1000 (Western Blot)	Cell Signaling	3504
Anti-STING	1:1000 (Western Blot)	Cell Signaling	13647
Anti-pSTING	1:1000 (Western Blot)	Cell Signaling	50907
Anti-pIRF	1:1000 (Western Blot)	Cell Signaling	29047
Anti-IRF	1:1000 (Western Blot)	Cell Signaling	11904
Anti-BAF	1:250 (Western Blot)	ProSci	4019

Anti-BAF	1:200 (Immunofluorescence)	Abcam	ab129184
DNA Construct			
pICE-FLAG-BANF1 (made by A. Janssen)	1 µg for 12-well 2 µg for 6-well		
pICE	1 µg for 12-well 2 µg for 6-well		
Chemical Agents			
Cyclohexamide	Final concentration 10 µM	Sigma Aldrich	01810
MG132	Final concentration 0.3 µM	Sigma Aldrich	1211877-36-9

CellProfiler™ Quantification Workflow

We used the CellProfiler™ software to carry out automated detection of quantification of nuclear phenotypes. To calculate the nuclear form factor, or intensity of different staining (including DAPI), the DAPI staining was first used to identify the nucleus, and secondary nuclear or cytoplasmic staining were identified for filtering or intensity measurements (**Table 2**).

To identify nuclear blebs, a separate CellProfiler™ pipeline was used (**Table 3**). In this pipeline, the nucleus is identified based on the DAPI staining, and the blebs are identified based on the difference in area between the DAPI and Lamin B staining. Both pipelines used were developed by Anne Janssen in the Larrieu Lab.

To assess and compare nuclear morphology quantitatively, we employed the CellProfiler™ software. Using this software, we developed pipelines that identifies nuclei, evaluates the nuclear morphology, and measures immunofluorescent intensities within different subcellular compartments.

In the first step of the pipeline, the nuclei were identified by their DAPI signal. To ensure the proper identification of nuclei, and exclusion of non-nuclear artifacts in the image such as micronuclei, we established lower and upper thresholds for the size of identified objects. For the images acquired at 63x magnification, we found that a range of 100 to 700 pixels to be suitable (**Table 2, Setting A**).

For WT cells stably expressing HA-CSA, we used HA antibodies to stain for HA-CSA in the DsRed channel and filtered the images through a threshold of HA signal. We found the

threshold value of 0.012 to work well, as shown by the resulting nuclei identified in **Table 2, Setting C**.

To measure morphological features of the nucleus, we utilised the “Measure Object Size and Shape” function, in which the previously identified nuclei were evaluated for their size and shape (**Table 2, Setting G**). The nuclear shape was measured by assigning a numerical score between 0 and 1. A score of 1 would indicate a perfect circle, while a score closer to 0 would indicate a nuclear shape that deviates further from the circular shape. Since most nuclei under normal physiological conditions take on an ovoidal morphology, the score tends to approach 0.8, although this varies depending on cell type and extracellular conditions. This function ultimately generated a Microsoft Excel sheet with a numerical score assigned to each identified nucleus. Data analysis could then be performed on this population of values.

To measure the intensity of nuclear and cytoplasmic immunofluorescent signals, we utilised the setting “Measure Object Intensity,” which identified the signal within a particular channel, and scored its intensity (**Table 2, Settings B, F**). Cytoplasmic signal was measured by first establishing a larger artificial area, a set number of pixels outward from the nuclear perimeter. We found 30 pixels to be sufficient (**Table 2, Setting D**). After identifying this “secondary object,” the area of the primary nucleus was subtracted from that of the secondary object, to establish a “tertiary object,” that constituted a “cytoplasmic ring” around the nucleus (**Table 2, Setting E**). The intensity of selected immunofluorescent signals could then be measured.

Table 2. CellProfiler™ quantification pipeline screenshots for nuclear form factor and immunofluorescence intensity.

Setting	Sample Images
A. Identify Primary Objects	<p>The screenshot shows the CellProfiler pipeline interface. On the left, a tree view lists modules: Images, Metadata, NamesAndTypes, Groups, IdentifyPrimaryObjects (which is selected and highlighted in grey), MeasureObjectIntensity, FilterObjects, IdentifySecondaryObjects, IdentifyTertiaryObjects, MeasureObjectIntensity, MeasureObjectSizeShape, MeasureObjectSizeShape, OverlayOutlines, SaveImages, and ExportToSpreadsheet. On the right, the 'IdentifyPrimaryObjects' module settings are displayed. It includes fields for 'Select the input image' (set to DNA), 'Name the primary objects to be identified' (set to Nuclei), 'Typical diameter of objects, in pixel units (Min,Max)' (set to 100, 700), 'Discard objects outside the diameter range?' (radio button set to Yes), and 'Discard objects touching the border of the image?' (radio button set to Yes). At the bottom, there are buttons for 'Output Settings', 'View Workspace', 'Adjust modules', 'Start Test Mode', and 'Analyze Images'. The status bar at the bottom right indicates 'Found 24 rows'.</p>

	<p>Input image, cycle #1</p> <p>Nuclei</p> <p>Nuclei outlines</p> <table border="1"> <tr><td># of accepted objects</td><td>31</td></tr> <tr><td>10th pctl diameter</td><td>122.0 pixels</td></tr> <tr><td>Median diameter</td><td>158.3 pixels</td></tr> <tr><td>90th pctl diameter</td><td>180.8 pixels</td></tr> <tr><td>Area covered by objects</td><td>15.0 %</td></tr> <tr><td>Thresholding filter size</td><td>1.0</td></tr> <tr><td>Threshold</td><td>0.0625</td></tr> <tr><td>Declumping smoothing filter size</td><td>67.1</td></tr> <tr><td>Maxima suppression size</td><td>70.0</td></tr> </table> <p>X: 1923 Y: 907 Intensity: 20</p>	# of accepted objects	31	10th pctl diameter	122.0 pixels	Median diameter	158.3 pixels	90th pctl diameter	180.8 pixels	Area covered by objects	15.0 %	Thresholding filter size	1.0	Threshold	0.0625	Declumping smoothing filter size	67.1	Maxima suppression size	70.0
# of accepted objects	31																		
10th pctl diameter	122.0 pixels																		
Median diameter	158.3 pixels																		
90th pctl diameter	180.8 pixels																		
Area covered by objects	15.0 %																		
Thresholding filter size	1.0																		
Threshold	0.0625																		
Declumping smoothing filter size	67.1																		
Maxima suppression size	70.0																		
B. Measure Object Intensity	<p>Module configuration for Measure Object Intensity:</p> <ul style="list-style-type: none"> Images, Metadata, NamesAndTypes, Groups IdentifyPrimaryObjects, MeasureObjectIntensity (selected), FilterObjects, IdentifySecondaryObjects, IdentifyTertiaryObjects, MeasureObjectIntensity, MeasureObjectSizeShape, OverlayOutlines, SaveImages, ExportToSpreadsheet <p>Output Settings, View Workspace, Adjust modules, Start Test Mode, Analyze Images, Found 24 rows.</p>																		
C. Filter Objects	<p>Module configuration for FilterObjects:</p> <ul style="list-style-type: none"> Images, Metadata, NamesAndTypes, Groups IdentifyPrimaryObjects, MeasureObjectIntensity, FilterObjects (selected), IdentifySecondaryObjects, IdentifyTertiaryObjects, MeasureObjectIntensity, MeasureObjectSizeShape, OverlayOutlines, SaveImages, ExportToSpreadsheet <p>Output Settings, View Workspace, Adjust modules, Start Test Mode, Analyze Images, Found 24 rows.</p>																		

	<p>Images Metadata NamesAndTypes Groups</p> <p><input checked="" type="checkbox"/> IdentifyPrimaryObjects <input checked="" type="checkbox"/> MeasureObjectIntensity <input checked="" type="checkbox"/> FilterObjects <input checked="" type="checkbox"/> IdentifySecondaryObjects <input checked="" type="checkbox"/> IdentifyTertiaryObjects <input checked="" type="checkbox"/> MeasureObjectSizeShape <input checked="" type="checkbox"/> MeasureObjectIntensity <input checked="" type="checkbox"/> OverlayOutlines <input checked="" type="checkbox"/> SaveImages <input checked="" type="checkbox"/> ExportToSpreadsheet</p> <p>Select the measurement to filter by Measurement: MeanIntensity Image: HACSA</p> <p>Filter using a minimum measurement value? Yes No Minimum value: 0.012</p> <p>Filter using a maximum measurement value? Yes No</p> <p>Add another measurement</p> <p>Output Settings View Workspace Adjust modules: + - ^ Start Test Mode Analyze Images Found 24 rows</p> <p>Original: Nuclei Filtered: CSAPositive</p> <p>Number of objects pre-filtering 31 Number of objects post-filtering 31</p>
D. Identify Secondary Objects	<p>Images Metadata NamesAndTypes Groups</p> <p><input checked="" type="checkbox"/> IdentifyPrimaryObjects <input checked="" type="checkbox"/> MeasureObjectIntensity <input checked="" type="checkbox"/> FilterObjects <input checked="" type="checkbox"/> IdentifySecondaryObjects <input checked="" type="checkbox"/> IdentifyTertiaryObjects <input checked="" type="checkbox"/> MeasureObjectSizeShape <input checked="" type="checkbox"/> MeasureObjectIntensity <input checked="" type="checkbox"/> OverlayOutlines <input checked="" type="checkbox"/> SaveImages <input checked="" type="checkbox"/> ExportToSpreadsheet</p> <p>Cytoplasm measurement based on propagation of a ring outward from the identified nucleus</p> <p>Select the input image: HACSA (from NamesAndTypes) Select the input objects: CSAPositive (from FilterObjects #07)</p> <p>Name the objects to be identified: Cells Select the method to identify the secondary objects: Distance - N Number of pixels by which to expand the primary objects: 30</p> <p>Fill holes in identified objects? Yes No Discard secondary objects touching the border of the image? Yes No</p> <p>Output Settings View Workspace Adjust modules: + - ^ Start Test Mode Analyze Images Found 24 rows</p>

E. Identify Tertiary Objects	<p>Module selection:</p> <ul style="list-style-type: none"> <input checked="" type="checkbox"/> Images <input checked="" type="checkbox"/> Metadata <input checked="" type="checkbox"/> NamesAndTypes <input checked="" type="checkbox"/> Groups <input checked="" type="checkbox"/> IdentifyPrimaryObjects <input checked="" type="checkbox"/> MeasureObjectIntensity <input checked="" type="checkbox"/> FilterObjects <input checked="" type="checkbox"/> IdentifySecondaryObjects <input checked="" type="checkbox"/> IdentifyTertiaryObjects <input checked="" type="checkbox"/> MeasureObjectSizeShape <input checked="" type="checkbox"/> OverlayOutlines <input checked="" type="checkbox"/> SaveImages <input checked="" type="checkbox"/> ExportToSpreadsheet <p>Configuration settings:</p> <ul style="list-style-type: none"> Select the larger identified objects: Cells (from identifySecondaryObjects #08) Select the smaller identified objects: Nuclei (from identifyPrimaryObjects #05) Name the tertiary objects to be identified: Cytoplasm Shrink smaller object prior to subtraction? <input type="radio"/> Yes <input checked="" type="radio"/> No <p>Output Settings: View Workspace Adjust modules: + - ^ ?</p> <p>Start Test Mode Analyze Images Found 24 rows</p>

F. Measure Object Intensity	<p>Module configuration:</p> <ul style="list-style-type: none"> <input checked="" type="checkbox"/> Images <input checked="" type="checkbox"/> Metadata <input checked="" type="checkbox"/> NamesAndTypes <input checked="" type="checkbox"/> Groups <input checked="" type="checkbox"/> IdentifyPrimaryObjects <input checked="" type="checkbox"/> MeasureObjectIntensity <input checked="" type="checkbox"/> FilterObjects <input checked="" type="checkbox"/> IdentifySecondaryObjects <input checked="" type="checkbox"/> IdentifyTertiaryObjects <input checked="" type="checkbox"/> MeasureObjectSizeShape <input checked="" type="checkbox"/> OverlayOutlines <input checked="" type="checkbox"/> SaveImages <input checked="" type="checkbox"/> ExportToSpreadsheet <p>Select images to measure:</p> <ul style="list-style-type: none"> <input checked="" type="checkbox"/> DNA (from NamesAndTypes) <input checked="" type="checkbox"/> HACSA (from NamesAndTypes) <p>Select objects to measure:</p> <ul style="list-style-type: none"> <input checked="" type="checkbox"/> CSAPositive (from FilterObjects #07) <input type="checkbox"/> Cells (from IdentifySecondaryObjects #08) <input checked="" type="checkbox"/> Cytoplasm (from IdentifyTertiaryObjects #09) <input checked="" type="checkbox"/> Nuclei (from IdentifyPrimaryObjects #05) <p>Output Settings View Workspace Adjust modules: + - ^ Start Test Mode Analyze Images Found 24 rows</p>
G. Measure Object Size and Shape	<p>Module configuration:</p> <ul style="list-style-type: none"> <input checked="" type="checkbox"/> Images <input checked="" type="checkbox"/> Metadata <input checked="" type="checkbox"/> NamesAndTypes <input checked="" type="checkbox"/> Groups <input checked="" type="checkbox"/> IdentifyPrimaryObjects <input checked="" type="checkbox"/> MeasureObjectIntensity <input checked="" type="checkbox"/> FilterObjects <input checked="" type="checkbox"/> IdentifySecondaryObjects <input checked="" type="checkbox"/> IdentifyTertiaryObjects <input checked="" type="checkbox"/> MeasureObjectSizeShape <input checked="" type="checkbox"/> OverlayOutlines <input checked="" type="checkbox"/> SaveImages <input checked="" type="checkbox"/> ExportToSpreadsheet <p>Select object sets to measure:</p> <ul style="list-style-type: none"> <input checked="" type="checkbox"/> CSAPositive (from FilterObjects #07) <input type="checkbox"/> Cells (from IdentifySecondaryObjects #08) <input checked="" type="checkbox"/> Cytoplasm (from IdentifyTertiaryObjects #09) <input checked="" type="checkbox"/> Nuclei (from IdentifyPrimaryObjects #05) <p>Calculate the Zernike features? <input type="radio"/> Yes <input checked="" type="radio"/> No</p> <p>Calculate the advanced features? <input type="radio"/> Yes <input checked="" type="radio"/> No</p> <p>Output Settings View Workspace Adjust modules: + - ^ Start Test Mode Analyze Images Found 24 rows</p>

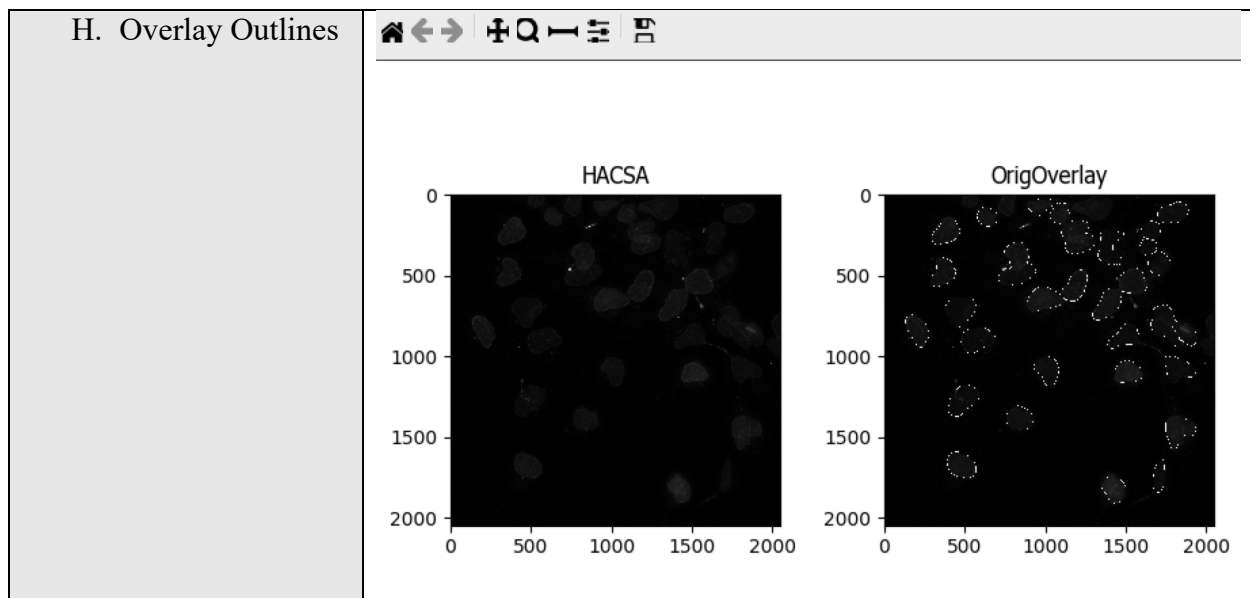


Table 3. CellProfiler™ quantification pipeline screenshots for nuclear bleb analysis.

Step	Images Illustrating Settings
Identify Primary Objects	<p>Images Metadata NamesAndTypes Groups</p> <p>IdentifyPrimaryObjects</p> <p>ExpandOrShrinkObjects</p> <p>IdentifyTertiaryObjects</p> <p>SplitOrMergeObjects</p> <p>MeasureObjectSizeShape</p> <p>FilterObjects</p> <p>MeasureObjectIntensity</p> <p>MeasureObjectSizeShape</p> <p>RelateObjects</p> <p>OverlayOutlines</p> <p>SaveImages</p> <p>ExportToSpreadsheet</p> <p>Output Settings View Workspace</p> <p>Adjust modules: + - ^ v</p> <p>Start Test Mode Analyze Images</p>

Images

Metadata

NamesAndTypes

Groups

IdentifyPrimaryObjects

IdentifyTertiaryObjects

ExpandOrShrinkObjects

SplitOrMergeObjects

MeasureObjectSizeShape

FilterObjects

MeasureObjectIntensity

MeasureObjectSizeShape

RelatedObjects

OverlayOutlines

SaveImages

ExportToSpreadsheet

Typical diameter of objects, in pixel units: 100 800
(Min,Max)

Discard objects outside the diameter range? Yes No

Discard objects touching the border of the image? Yes No

Threshold strategy: Global

Thresholding method: Minimum Cross-Entropy

Threshold smoothing scale: 1.3488

Threshold correction factor: 1.0

Lower and upper bounds on threshold: 0.0 1.0

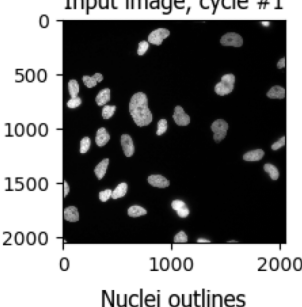
Log transform before thresholding? Yes No

Method to distinguish clumped objects: None

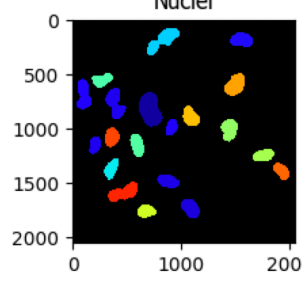
Fill holes in identified objects? After declumping only

Handling of objects if excessive number of objects identified: Continue

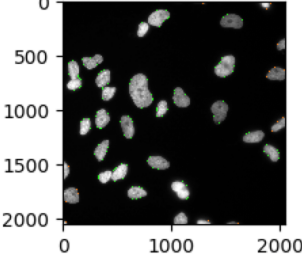
Input image, cycle #1



Nuclei



Nuclei outlines



# of accepted objects	20
10th pctl diameter	141.8 pixels
Median diameter	163.7 pixels
90th pctl diameter	212.5 pixels
Area covered by objects	11.2 %
Thresholding filter size	1.0
Threshold	0.148

Identify Primary Objects

Images

Metadata

NamesAndTypes

Groups

IdentifyPrimaryObjects

IdentifyTertiaryObjects

ExpandOrShrinkObjects

SplitOrMergeObjects

MeasureObjectSizeShape

FilterObjects

MeasureObjectIntensity

MeasureObjectSizeShape

RelatedObjects

OverlayOutlines

SaveImages

ExportToSpreadsheet

No declumping used as this sometimes led to separation of nuclei in multiple objects. Threshold factor increased to 1.1 to avoid inclusion of low laminB regions (blebs) in mask.

Use advanced settings? Yes No

Select the input image: laminB (from NamesAndTypes)

Name the primary objects to be identified: laminB

Typical diameter of objects, in pixel units: 100 800
(Min,Max)

Discard objects outside the diameter range? Yes No

Discard objects touching the border of the image? Yes No

Threshold strategy: Global

Thresholding method: Minimum Cross-Entropy

Threshold smoothing scale: 1.3488

Threshold correction factor: 1.1

Lower and upper bounds on threshold: 0.0 1.0

Log transform before thresholding? Yes No

Method to distinguish clumped objects: None

IdentifyPrimaryObjects

- Images
- Metadata
- NamesAndTypes
- Groups
- IdentifyPrimaryObjects
- ExpandOrShrinkObjects
- IdentifyTertiaryObjects
- SplitOrMergeObjects
- MeasureObjectSizeShape
- FilterObjects
- MeasureObjectIntensity
- MeasureObjectSizeShape
- RelatedObjects
- OverlayOutlines
- SaveImages
- ExportToSpreadsheet

No declumping used as this sometimes led to separation of nuclei in multiple objects. Threshold factor increased to 1.1 to avoid inclusion of low laminB regions (blebs) in mask.

Name the primary objects to be identified: **laminB**

Typical diameter of objects, in pixel units (Min,Max): 100 800

Discard objects outside the diameter range? Yes No

Discard objects touching the border of the image? Yes No

Threshold strategy: Global

Thresholding method: Minimum Cross-Entropy

Threshold smoothing scale: 1.3488

Threshold correction factor: 1.1

Lower and upper bounds on threshold: 0.0 1.0

Log transform before thresholding? Yes No

Method to distinguish clumped objects: None

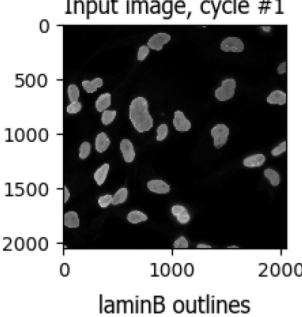
Fill holes in identified objects? After both thresholding and declumping

Handling of objects if excessive number of objects identified: Continue

Output Settings **View Workspace**

Start Test Mode **Analyze Images** Found 3 rows

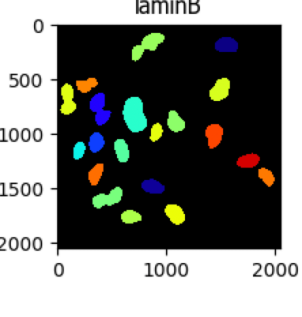
Input image, cycle #1



0
500
1000
1500
2000

0 1000 2000

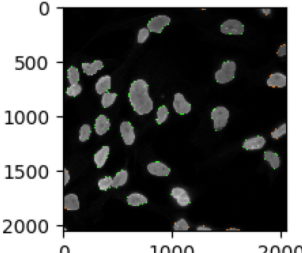
laminB



0
500
1000
1500
2000

0 1000 2000

laminB outlines



0
500
1000
1500
2000

0 1000 2000

# of accepted objects	20
10th pctlle diameter	146.6 pixels
Median diameter	170.3 pixels
90th pctlle diameter	214.7 pixels
Area covered by objects	11.9 %
Thresholding filter size	1.0
Threshold	0.132

Expand or Shrink Objects

ExpandOrShrinkObjects

- Images
- Metadata
- NamesAndTypes
- Groups
- IdentifyPrimaryObjects
- IdentifyPrimaryObjects
- ExpandOrShrinkObjects
- IdentifyTertiaryObjects
- SplitOrMergeObjects
- MeasureObjectSizeShape
- FilterObjects
- MeasureObjectIntensity
- MeasureObjectSizeShape
- RelatedObjects
- OverlayOutlines
- SaveImages
- ExportToSpreadsheet

Expand laminB mask to avoid edge pixels not included in DAPI mask

Select the input objects: **laminB** (from IdentifyPrimaryObjects #06)

Name the output objects: **laminBexpanded**

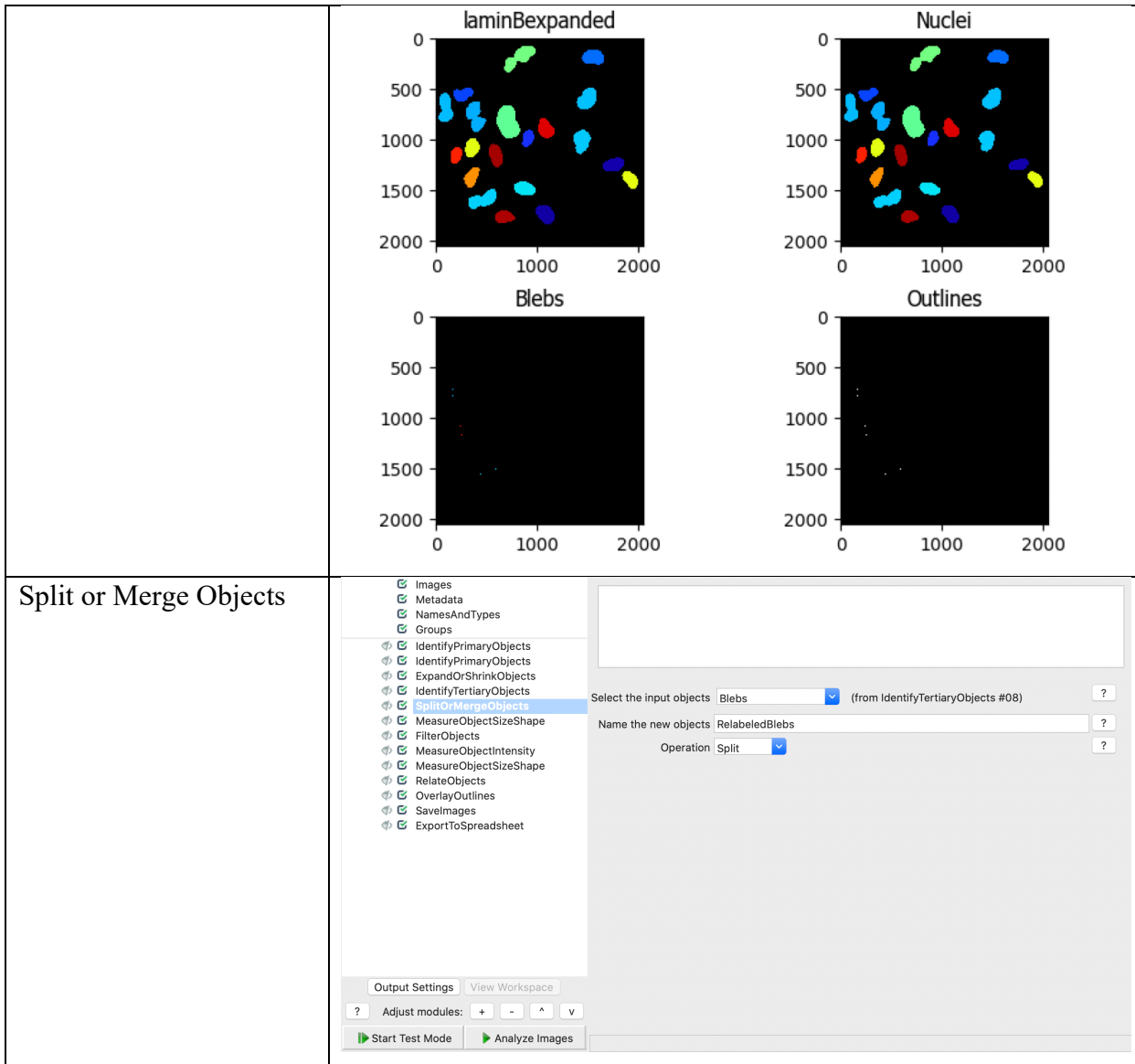
Select the operation: **Expand objects by a specified number of pixels**

Number of pixels by which to expand or shrink: 3

Output Settings **View Workspace**

Start Test Mode **Analyze Images**

Identify Tertiary Objects	<p>Module configuration:</p> <ul style="list-style-type: none"> <input checked="" type="checkbox"/> Images <input checked="" type="checkbox"/> Metadata <input checked="" type="checkbox"/> NamesAndTypes <input checked="" type="checkbox"/> Groups <input checked="" type="checkbox"/> IdentifyPrimaryObjects <input checked="" type="checkbox"/> IdentifyPrimaryObjects <input checked="" type="checkbox"/> ExpandOrShrinkObjects <input checked="" type="checkbox"/> IdentifyTertiaryObjects <input checked="" type="checkbox"/> SplitOrMergeObjects <input checked="" type="checkbox"/> MeasureObjectSizeShape <input checked="" type="checkbox"/> FilterObjects <input checked="" type="checkbox"/> MeasureObjectIntensity <input checked="" type="checkbox"/> MeasureObjectSizeShape <input checked="" type="checkbox"/> RelateObjects <input checked="" type="checkbox"/> OverlayOutlines <input checked="" type="checkbox"/> SaveImages <input checked="" type="checkbox"/> ExportToSpreadsheet <p>Parameter settings:</p> <ul style="list-style-type: none"> Select the larger identified objects: Nuclei (from IdentifyPrimaryObjects #05) Select the smaller identified objects: laminBexpanded (from ExpandOrShrinkObjects #07) Name the tertiary objects to be identified: Blebs Shrink smaller object prior to subtraction? <input checked="" type="radio"/> No <p>Output Settings: View Workspace</p> <p>Adjust modules: + - ^ v</p> <p>Start Test Mode Analyze Images</p>



Measure Object Size and Shape	<p>Module interface for 'Measure Object Size and Shape'.</p> <ul style="list-style-type: none"> <input checked="" type="checkbox"/> Images <input checked="" type="checkbox"/> Metadata <input checked="" type="checkbox"/> NameAndTypes <input checked="" type="checkbox"/> Groups <input checked="" type="checkbox"/> IdentifyPrimaryObjects <input checked="" type="checkbox"/> IdentifyTertiaryObjects <input checked="" type="checkbox"/> ExpandOrShrinkObjects <input checked="" type="checkbox"/> SplitOrMergeObjects <input checked="" type="checkbox"/> MeasureObjectSizeShape (selected) <input checked="" type="checkbox"/> FilterObjects <input checked="" type="checkbox"/> MeasureObjectIntensity <input checked="" type="checkbox"/> MeasureObjectSizeShape <input checked="" type="checkbox"/> RelateObjects <input checked="" type="checkbox"/> OverlayOutlines <input checked="" type="checkbox"/> SaveImages <input checked="" type="checkbox"/> ExportToSpreadsheet <p>Select object sets to measure:</p> <table border="1"> <tr> <td><input type="checkbox"/> Blebs</td> <td>(from IdentifyTerti...</td> <td>?</td> </tr> <tr> <td><input type="checkbox"/> Nuclei</td> <td>(from IdentifyPrim...</td> <td>?</td> </tr> <tr> <td><input checked="" type="checkbox"/> RelabeledBlebs</td> <td>(from SplitOr...</td> <td>?</td> </tr> <tr> <td><input type="checkbox"/> laminB</td> <td>(from IdentifyPrim...</td> <td>?</td> </tr> <tr> <td><input type="checkbox"/> laminExpanded</td> <td>(from Expan...</td> <td>?</td> </tr> </table> <p>Calculate the Zernike features? <input type="radio"/> Yes <input checked="" type="radio"/> No ?</p> <p>Calculate the advanced features? <input type="radio"/> Yes <input checked="" type="radio"/> No ?</p> <p>Output Settings View Workspace</p> <p>Adjust modules: + - ^ v</p> <p>Start Test Mode Analyze Images</p>	<input type="checkbox"/> Blebs	(from IdentifyTerti...	?	<input type="checkbox"/> Nuclei	(from IdentifyPrim...	?	<input checked="" type="checkbox"/> RelabeledBlebs	(from SplitOr...	?	<input type="checkbox"/> laminB	(from IdentifyPrim...	?	<input type="checkbox"/> laminExpanded	(from Expan...	?
<input type="checkbox"/> Blebs	(from IdentifyTerti...	?														
<input type="checkbox"/> Nuclei	(from IdentifyPrim...	?														
<input checked="" type="checkbox"/> RelabeledBlebs	(from SplitOr...	?														
<input type="checkbox"/> laminB	(from IdentifyPrim...	?														
<input type="checkbox"/> laminExpanded	(from Expan...	?														
Filter Objects																

Original: RelabeledBlebs

Filtered: FilteredBlebs

Number of objects pre-filtering	34
Number of objects post-filtering	0

Output Settings View Workspace
? Adjust modules: + - ^ v
Start Test Mode Analyze Images

Images
Metadata
NamesAndTypes
Groups
IdentifyPrimaryObjects
IdentifyTertiaryObjects
ExpandOrShrinkObjects
MeasureObjectIntensity
MeasureObjectSizeShape
FilterObjects
RelateObjects
OverlayOutlines
SaveImages
ExportToSpreadsheet

Select the objects to filter RelabeledBlebs (from SplitOrMergeObjects #09)
Name the output objects FilteredBlebs

Select the filtering mode Measurements
Select the filtering method Limits
Select the measurement to filter Category: AreaShape by Measurement: Area

Filter using a minimum measurement value? Yes No
Minimum value: 200

Filter using a maximum measurement value? Yes No
Maximum value: 10000

Category: AreaShape

Filter using a maximum measurement value? Yes No
Maximum value: 10000

Select the measurement to filter Category: AreaShape by Measurement: FormFactor

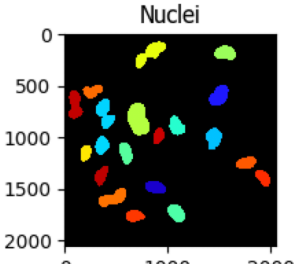
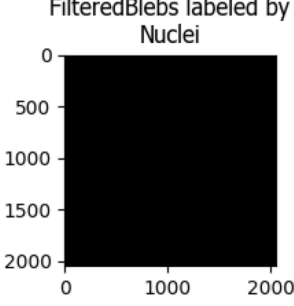
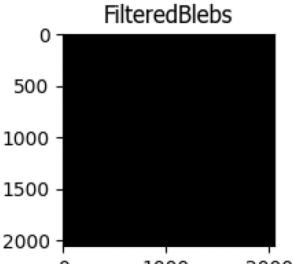
Filter using a minimum measurement value? Yes No
Minimum value: 0.15

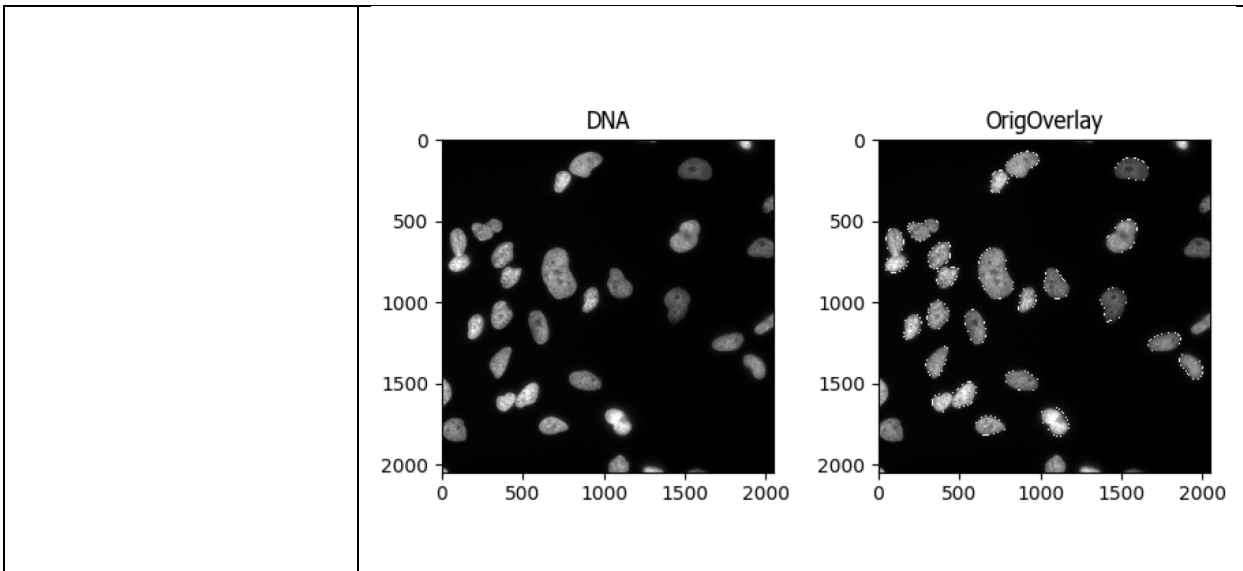
Filter using a maximum measurement value? Yes No
Maximum value: 10000

Add another measurement

Relabel additional objects to Add an additional object
match the filtered object?

Measure Object Intensity	<p>Module tree:</p> <ul style="list-style-type: none"> <input checked="" type="checkbox"/> Images <input checked="" type="checkbox"/> Metadata <input checked="" type="checkbox"/> NamesAndTypes <input checked="" type="checkbox"/> Groups <input checked="" type="checkbox"/> IdentifyPrimaryObjects <input checked="" type="checkbox"/> IdentifyPrimaryObjects <input checked="" type="checkbox"/> ExpandOrShrinkObjects <input checked="" type="checkbox"/> IdentifyTertiaryObjects <input checked="" type="checkbox"/> SplitOrMergeObjects <input checked="" type="checkbox"/> MeasureObjectSizeShape <input checked="" type="checkbox"/> FilterObjects <input checked="" type="checkbox"/> MeasureObjectIntensity <input checked="" type="checkbox"/> MeasureObjectSizeShape <input checked="" type="checkbox"/> RelateObjects <input checked="" type="checkbox"/> OverlayOutlines <input checked="" type="checkbox"/> SaveImages <input checked="" type="checkbox"/> ExportToSpreadsheet <p>Select images to measure:</p> <ul style="list-style-type: none"> <input type="checkbox"/> DNA (from NamesAndT...) <input checked="" type="checkbox"/> LAP2 (from NamesAndT...) <input checked="" type="checkbox"/> laminB (from NamesAndT...) <p>Select objects to measure:</p> <ul style="list-style-type: none"> <input type="checkbox"/> Blebs (from IdentifyTertiaryObject...) <input checked="" type="checkbox"/> FilteredBlebs (from FilterObject...) <input checked="" type="checkbox"/> Nuclei (from IdentifyPrimaryObject...) <input type="checkbox"/> RelabeledBlebs (from SplitOrMergeObject...) <input checked="" type="checkbox"/> laminB (from IdentifyPrimaryObject...) <input type="checkbox"/> laminBexpanded (from ExpandOrShr...) <p>Output Settings View Workspace ? Adjust modules: + - ^ v Start Test Mode Analyze Images</p>
Measure Object Size and Shape	<p>Module tree:</p> <ul style="list-style-type: none"> <input checked="" type="checkbox"/> Images <input checked="" type="checkbox"/> Metadata <input checked="" type="checkbox"/> NamesAndTypes <input checked="" type="checkbox"/> Groups <input checked="" type="checkbox"/> IdentifyPrimaryObjects <input checked="" type="checkbox"/> IdentifyPrimaryObjects <input checked="" type="checkbox"/> ExpandOrShrinkObjects <input checked="" type="checkbox"/> IdentifyTertiaryObjects <input checked="" type="checkbox"/> SplitOrMergeObjects <input checked="" type="checkbox"/> MeasureObjectSizeShape <input checked="" type="checkbox"/> FilterObjects <input checked="" type="checkbox"/> MeasureObjectIntensity <input checked="" type="checkbox"/> MeasureObjectSizeShape <input checked="" type="checkbox"/> RelateObjects <input checked="" type="checkbox"/> OverlayOutlines <input checked="" type="checkbox"/> SaveImages <input checked="" type="checkbox"/> ExportToSpreadsheet <p>Select object sets to measure:</p> <ul style="list-style-type: none"> <input type="checkbox"/> Blebs (from IdentifyTertiaryObject...) <input checked="" type="checkbox"/> FilteredBlebs (from FilterObject...) <input type="checkbox"/> Nuclei (from IdentifyPrimaryObject...) <input type="checkbox"/> RelabeledBlebs (from SplitOrMergeObject...) <input type="checkbox"/> laminB (from IdentifyPrimaryObject...) <input type="checkbox"/> laminBexpanded (from ExpandOrShr...) <p>Calculate the Zernike features? <input type="radio"/> Yes <input checked="" type="radio"/> No</p> <p>Calculate the advanced features? <input type="radio"/> Yes <input checked="" type="radio"/> No</p> <p>Output Settings View Workspace ? Adjust modules: + - ^ v Start Test Mode Analyze Images</p>
Relate Shape	<p>Module tree:</p> <ul style="list-style-type: none"> <input checked="" type="checkbox"/> Images <input checked="" type="checkbox"/> Metadata <input checked="" type="checkbox"/> NamesAndTypes <input checked="" type="checkbox"/> Groups <input checked="" type="checkbox"/> IdentifyPrimaryObjects <input checked="" type="checkbox"/> IdentifyPrimaryObjects <input checked="" type="checkbox"/> ExpandOrShrinkObjects <input checked="" type="checkbox"/> IdentifyTertiaryObjects <input checked="" type="checkbox"/> SplitOrMergeObjects <input checked="" type="checkbox"/> MeasureObjectSizeShape <input checked="" type="checkbox"/> FilterObjects <input checked="" type="checkbox"/> MeasureObjectIntensity <input checked="" type="checkbox"/> MeasureObjectSizeShape <input checked="" type="checkbox"/> RelateObjects <input checked="" type="checkbox"/> OverlayOutlines <input checked="" type="checkbox"/> SaveImages <input checked="" type="checkbox"/> ExportToSpreadsheet <p>Parent objects: Nuclei (from IdentifyPrimaryObjects #05)</p> <p>Child objects: FilteredBlebs (from FilterObjects #11)</p> <p>Calculate per-parent means for all child measurements? <input type="radio"/> Yes <input checked="" type="radio"/> No</p> <p>Calculate child-parent distances? None</p> <p>Do you want to save the children with parents as a new object set? <input type="radio"/> Yes <input checked="" type="radio"/> No</p> <p>Output Settings View Workspace ? Adjust modules: + - ^ v Start Test Mode Analyze Images</p>

	 <p>Nuclei</p>  <p>FilteredBlebs labeled by Nuclei</p>	 <p>FilteredBlebs</p>
Overlay Outlines	<p>Images Metadata NamesAndTypes Groups</p> <p>IdentifyPrimaryObjects IdentifyTertiaryObjects ExpandOrShrinkObjects SplitOrMergeObjects MeasureObjectSizeShape FilterObjects MeasureObjectIntensity MeasureObjectSizeShape OverlayOutlines SaveImages ExportToSpreadsheet</p> <p>Display outlines on a blank image? <input type="radio"/> Yes <input checked="" type="radio"/> No</p> <p>Select image on which to display DNA (from NamesAndTypes)</p> <p>Name the output image OrigOverlay</p> <p>Outline display mode Grayscale</p> <p>How to outline Thick</p> <p>Select method to determine brightness of outlines Max possible</p> <p>Select objects to display FilteredBlebs (from FilterObjects #11)</p> <p>Select objects to display Nuclei (from IdentifyPrimaryObjects #05)</p> <p>Remove this outline Add another outline</p> <p>Output Settings View Workspace</p> <p>? Adjust modules: + - ^ v</p> <p>Start Test Mode Analyze Images</p>	



Proliferation Assay

For proliferation assays, CS-A and WT cells were seeded at a similar confluence and transfected with control or FLAG-BAF DNA construct in 24-well plates. Plates were then transferred into an IncuCyte ® S3 Live-Cell Analysis System (Essen BioScience). Phase-contrast images were acquired every 4 hours over a period of 48 hours. Percentage of cell confluence was calculated using the Cell Player integrated software (Essen BioScience) and analysed with GraphPad Prism®.

Statistical analysis

All statistical analysis was performed on Prism®, unless stated otherwise. For experiments performed in triplicate ($n=3$) where no statistical analysis is performed, such as with the IncuCyte ® Live-Cell proliferation analysis, one representative graph is shown.

RESULTS

Loss of CSA results in aberrant nuclear morphology.

To begin investigating whether CSA or CSB plays a role in the maintenance of nuclear envelope integrity, other members of the lab had previously examined the effects of the knockout of *ERCC8* (CSA KO) and *ERCC6* (CSB KO) in the haploid HAP-1 cells. Compared to the control wildtype (WT) cells, CSA KO cells showed noticeable deformation of the nucleus, whereas CSB KO cells were morphologically similar to WT (**Figure 6A**).

To explore this phenotype further, we used Cockayne Syndrome patient-derived fibroblasts. First, the CSA patient cell line, (CS3BE henceforth called CS-A), harbours a homozygous missense mutation in *ERCC8* that results in a trp361cys substitution, and the loss of function mutation in CSA seen in these patients (Nardo et al., 2009). CS-A cells stably expressing HA-CSA (**Figure 6B**) will be used as control cells, which will hereafter be called WT. Additionally, we used a CSB patient cell line, (CS1AN henceforth called CS-B), in which a C-to-T transition led to the deletion of a portion of exon 13 (Troelstra et al., 1992). With this CS-B cell line, we generated complemented cells that stably express HA-GFP-CSB construct, which we labelled as WT-B. Notably, the level of HA-CSA in WT cells is significantly higher than the endogenous levels of CSA in CS-B patients (**Figure 6B**).

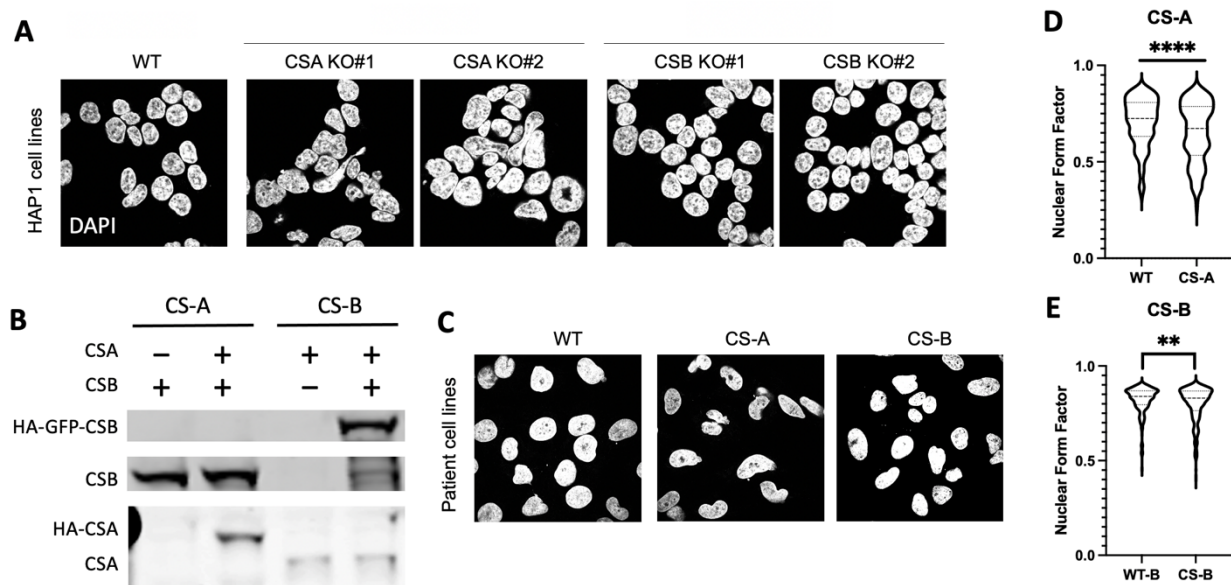


Figure 6. Loss of CSA but not CSB results in aberrant nuclear morphology. (A) Representative images (obtained by Delphine Larrieu) of DAPI-stained nuclei of HAP-1 cell lines

WT, with *ERCC8* knockout (CSA KO#1 and #2), and *ERCC6* knockout (CSB KO#1 and #2) (**B**) Western blotting analysis of WT, CS-A and CS-B cells using antibodies against CSB and CSA. (**C**) Representative images of DAPI-stained nuclei for WT, CS-A and CS-B cells. Automated quantification of the nuclear form factor using the Cell Profiler software in (**D**) WT (n = 358) and CS-A (n = 328) from 3 independent experiments *** P< 0.0001 (two-tailed unpaired t-test) and (**E**) WT-B (n = 248) and CS-B (n = 449) from 3 independent experiments. ** P<0.005 (Two-tailed unpaired t test).

Compared to WT, CS-A cells displayed a significant decrease in nuclear “roundness” (form factor, **Figure 6C, D**). While there was a decrease in nuclear form factor in CS-B cells, the average nuclear form factor was drastically higher than that of CS-A, and the reduction in form factor, when compared to WT-B, was less significant (**Figure 6E**). We therefore decided to focus on further examining CS-A cell phenotypes.

Loss of CSA decreases intensity of DAPI signal.

In examining the DAPI staining of WT and CS-A cells, we observed a reduced intensity of DAPI in the CS-A cells (**Figure 7A, B**). This decrease in DAPI signal may suggest a global de-condensation of chromatin but this would require further analysis and currently, the significance of this observation is unknown.

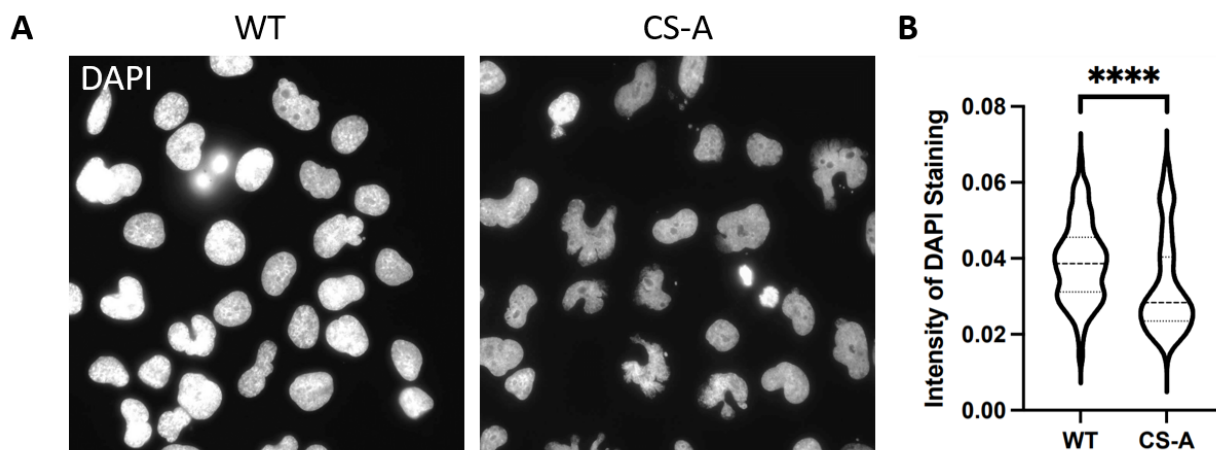


Figure 7. Loss of CSA reduces the intensity of DAPI staining. (**A**) Representative images of DAPI-stained nuclei for WT and CS-A cell lines. (**B**) Intensity of DAPI staining was measured

using Cell Profiler. Values of intensity were compiled for WT ($n = 223$) and CS-A ($n= 223$) from 3 independent experiments. The two population of data were compared via two-tailed unpaired t test. p-value *** $p < 0.0001$.

Loss of CSA increases the formation of nuclear blebs and micronuclei.

The initial observation of nuclear shape defects in CS-A cells suggested that the integrity of the nuclear envelope might be affected. To address this question, we assessed the prevalence of nuclear blebs in CS-A cells. Nuclear blebs are the outward protrusions of nuclear membranes, formed by the detachment of the nuclear membrane from the nuclear lamina. These nuclear blebs are especially susceptible to the rupture of the membrane, exposing the genomic material to the cytoplasm thereby challenging genomic integrity. To visualise the nuclear blebs, we stained the WT and CS-A nuclei with Lamin B and DAPI (Figure 8A). Lamin B has been previously shown to be absent from nuclear blebs (Chen et al., 2018). Thus, the combination of Lamin B and DAPI staining allows for the identification of nuclear blebs. The number of nuclei with one or more nuclear blebs was quantified and normalised to the number observed in WT cells. We saw that the loss of CSA increased the nuclear blebs frequency from 2.5-times to 10-times compared to WT cells (Figure 8B). It is important to note that in one of the experiments, cells were treated with control siRNA. While this should not affect the prevalence of nuclear abnormalities, further replicates may need to be done without siRNA. This result thus preliminarily suggest that the loss of CSA increases the formation of nuclear blebs.

In addition to nuclear blebs, the formation of micronuclei (MN) is another common nuclear aberration. MN are small-sized nuclear fragments formed from lagging chromosomal DNA. These MN form as a consequence of mitotic defects (Mackenzie et al., 2017; Ye et al., 2019). We observed an average of 50% increase in the number of micronuclei formed per nucleus (Figure 8C). Together, these results suggest that CSA plays a role in maintaining nuclear integrity.

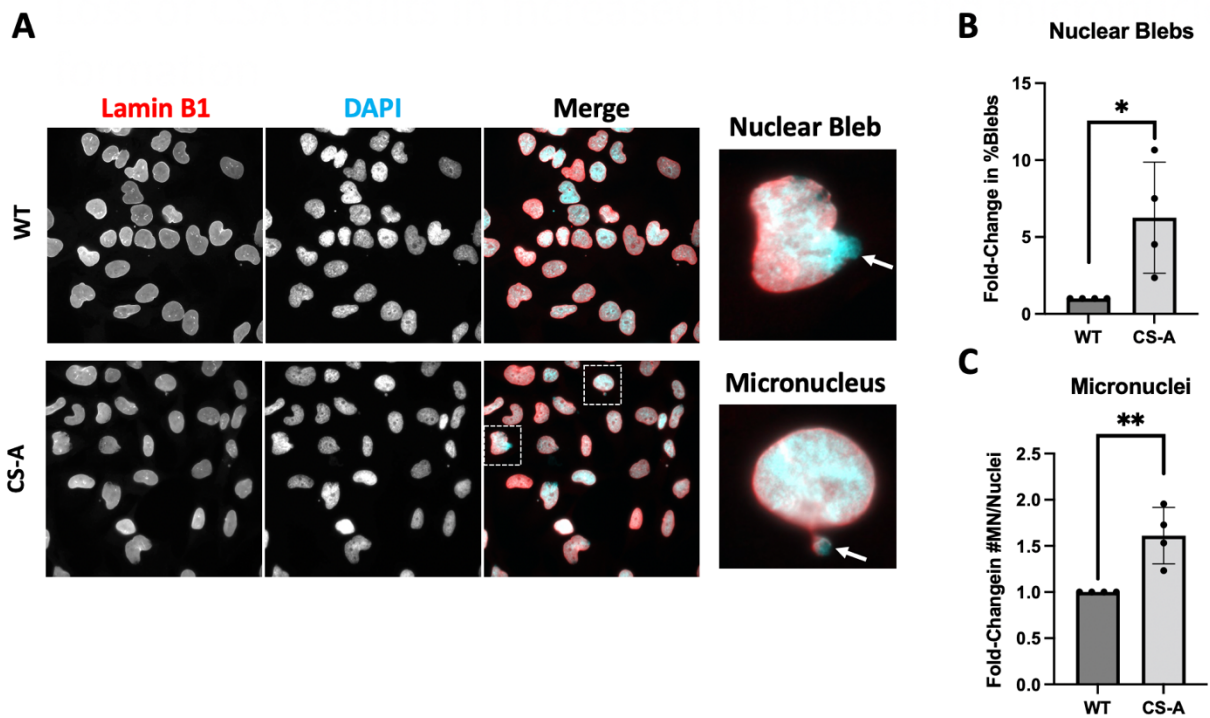


Figure 8. Loss of CSA increases formation of nuclear blebs and micronuclei. (A) Representative images of WT and CS-A nuclei stained with Lamin B1, DAPI, and merged. Insets show a representative image of nuclear bleb and a micronucleus, indicated by the white arrows. (B) Quantification of the fold-change in the percentage of nuclear blebs from 4 independent experiments. WT and CS-A was compared via two-tailed unpaired t test. * $p = 0.0268$. For WT cells, 94, 154, 161, 245 nuclei were evaluated in each experiment. For CS-A cells, 78, 151, 279, 207 nuclei were evaluated in each experiment. (C) Quantification of the fold change in the number of micronuclei from 4 independent experiments. WT and CS-A was compared via two-tailed unpaired t test. ** $p = 0.0071$. For WT cells, 57, 116, 161, 185 nuclei were assessed. For CS-A cells, 75, 116, 153, 125 nuclei were assessed.

Loss of CSA results in NE ruptures and activation of the cGAS/STING pathway.

Rupture of the nuclear envelope occurring from the sites of blebs or rupture of MN due to abnormal nuclear envelope integrity can lead to exposure of chromosomal or micronuclear DNA into the cytoplasm and activation of the innate immune cGAS-STING pathway (Mackenzie et al., 2017). Cyclic GMP-AMP synthase (cGAS) is a predominantly cytosolic DNA sensor in the cell. Upon binding to DNA, cGAS becomes activated, and triggers the phosphorylation-induced

activation of downstream effectors of the cGAS-STING signalling pathway, ultimately upregulating the interferon I response upon binding to DNA (Zierhut and Funabiki, 2020). It has been previously shown that nuclear envelope ruptures result in the local accumulation of cGAS (Zierhut and Funabiki, 2020) (**Figure 9A**). Therefore, to assess the presence of nuclear envelope ruptures in CS-A cells, we analysed the number of cGAS “foci” by immunofluorescence, normalised to the number of nuclei. We saw a significantly higher frequency of cGAS foci in CS-A cells compared to WT (**Figure 9B, C**). This suggests that the loss of CSA results in increased nuclear envelope ruptures. Accordingly, using western blotting analysis, we observed the activation of the cGAS/STING pathway in CS-A cells. Indeed, the level of cGAS, as well as the phosphorylation of its downstream effectors STING, IRF, and TBK were all increased. (**Figure 9D, E**).

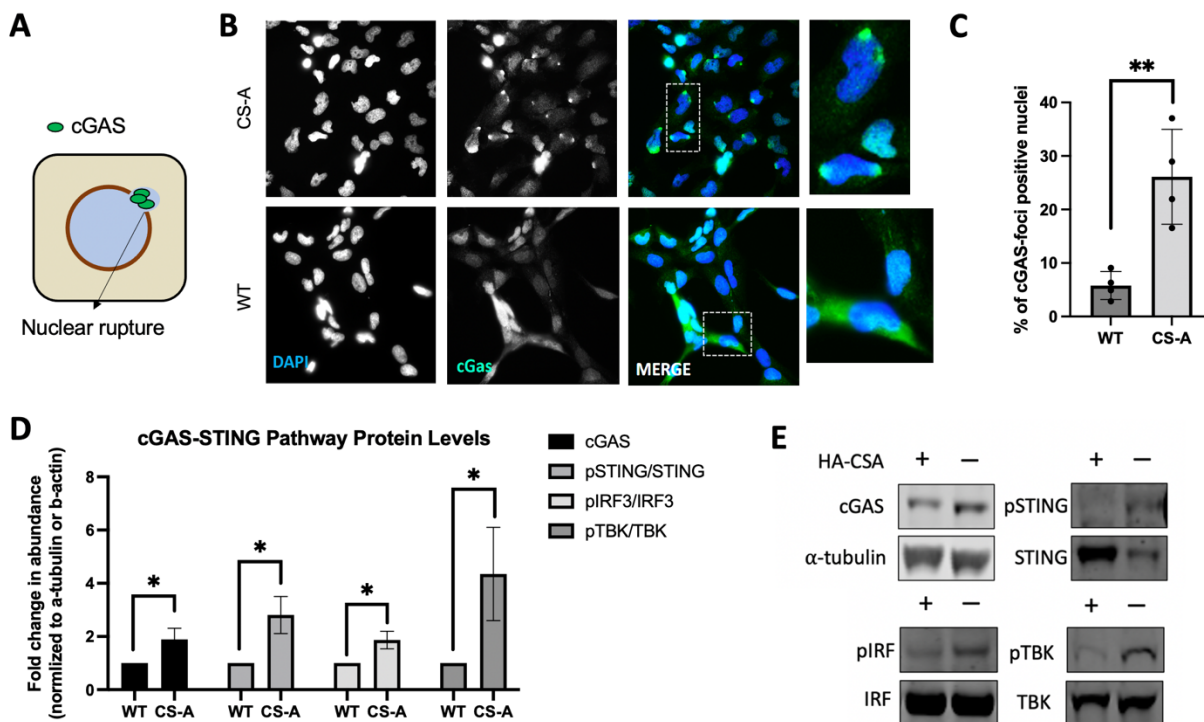


Figure 9. Loss of CSA results in nuclear envelope ruptures and activation of the cGAS/STING pathway. (A) Schematic of perinuclear cGAS aggregation as a marker for nuclear rupture. Ruptured nuclear envelope leads to recruitment of cGAS that binds to the exposed chromatin at the site of rupture. Adopted from (Zierhut and Funabiki, 2020). (B) Representative

immunofluorescence images of DAPI, cGAS, and merged signals in CS-A and WT. (C) cGAS aggregation was normalised to the number of nuclei to calculate the percentage of cGAS-aggregation positive nuclei. The two populations of data from 4 independent experiments were compared via two-tailed unpaired t test p-value (**p = 0.0046). For WT cells, 76, 81, 302, and 82 nuclei were evaluated in each replicate. For CS-A cells, 61, 66, 261, and 70 nuclei were evaluated in each replicate. (D) Quantification of western blotting data from 3 independent experiments as shown in (E) cGAS-STING pathway protein levels are expressed as mean ± S.D. (n = 3). The values were compared via two-tailed unpaired t test (Left to right, *p = 0.0210, 0.0108, 0.0107, 0.0296). (E) Representative immunoblot images of cGAS-STING pathway proteins.

CSA does not interact with core NE proteins and does not modulate their levels or localisation.

CSA is known to be part of an E3 ubiquitin ligase complex together with damage-binding protein 1 (DDB1) and Cullin4A (Groisman et al., 2003). Recently, the LEM Domain Nuclear Envelope Protein 2 (LEMD2) was also found to interact with DDB1 and Cullin4A (Moser et al., 2020). We therefore hypothesised that LEML2 might be the protein connecting CSA to the nuclear envelope. To explore whether the loss of CSA might affect the level of LEML2, we performed a western blotting and analysed several other core NE components including Lamin A, Lamin C, and Lamin B1. We saw no difference in the levels of these proteins between CS-A and WT cells (Figure 10A).

Immunofluorescence experiments showed no major changes in the localisation of lamin A/C, lamin B, and emerin (Figure 10B). Due to the difficulty in visualising LEML2 under normal conditions, we sought to reduce the background signal by treating the cells with the cytoskeleton buffer (CSK), which is a detergent mixture commonly used to release soluble proteins before immunofluorescence staining (Britton et al., 2013; Cramer and Mitchison, 1995). Under this condition, CS-A cells showed a noticeable reduction in the intensity of LEML2, suggesting a lower abundance of insoluble (and presumably membrane-associated) fraction. Further replicates would need to be done to test this in a statistically rigorous manner and explore its functional relevance to the observed nuclear defects in CS-A cells.

To explore whether CSA might interact with LEML2 and be part of the same DDB1/Cullin4A complex, we performed HA-CSA immunoprecipitation experiments. As a

positive control, we probed for CSB which is a known interactor of CSA and could indeed see that CSA co-immunoprecipitates with CSB. However, we could not detect any interaction between CSA and the nuclear envelope components Lamin A, Lamin C, or LEMD2 (**Figure 10C**). It is important to note that nuclear envelope proteins, like other membrane associated proteins, are highly insoluble and difficult to be isolated in through traditional immunoprecipitation technique. Furthermore, the report by Moser and colleagues identifying the interaction between LEMD2 and CSA interactors employed the biotinylation based BioID technique, which detects transient interactions.

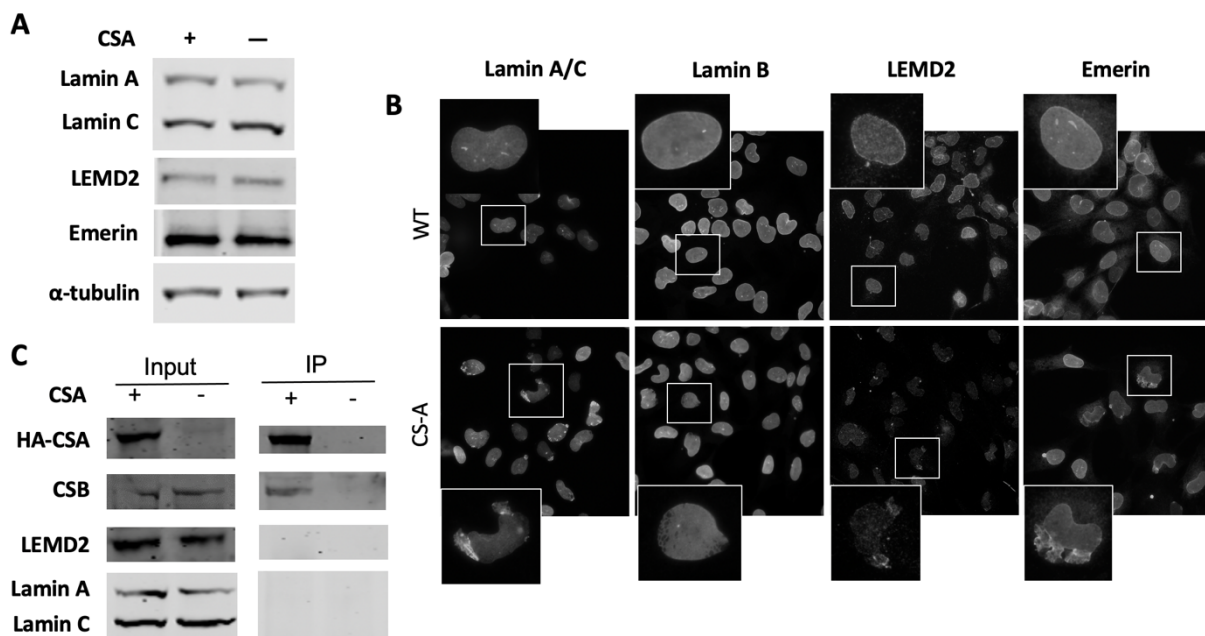


Figure 10. CSA does not alter levels and localisation of multiple nuclear envelope (NE) proteins or interacts with NE proteins. (A) Representative immunoblot showing the levels of Lamin A and C, LEMD2, Emerin, in WT and CS-A cells. α -tubulin was used as a loading control. (B) Representative immunofluorescence images of WT and CS-A cells stained for Lamin A/C, Lamin B, LEMD2, and Emerin. (C) Immunoprecipitation experiment was performed on CS-A and WT cells using HA-conjugated magnetic beads to pulldown HA-CSA and its interactors.

Loss of CSA results in decreased barrier-to-autointegration factor (BAF) levels.

As CS-A cells showed an increased number of nuclear envelope ruptures, we decided to investigate the levels of the barrier-to-autointegration factor 1 (BAF), a protein recently reported to play a role in nuclear envelope rupture repair (Halfmann et al., 2019). Interestingly, we found that CS-A cells expressed only approximately half of the levels of BAF compared to WT (**Figure 11A**). To confirm that this result was not cell type specific, we performed western blotting analysis of BAF levels in HAP-1 CSA KO cells and in CSA KO fibroblasts, supporting the result we obtained in patient cells (**Figure 11B, C**). Together, these provided robust evidence that the loss of CSA strongly reduces the steady-state levels of BAF.

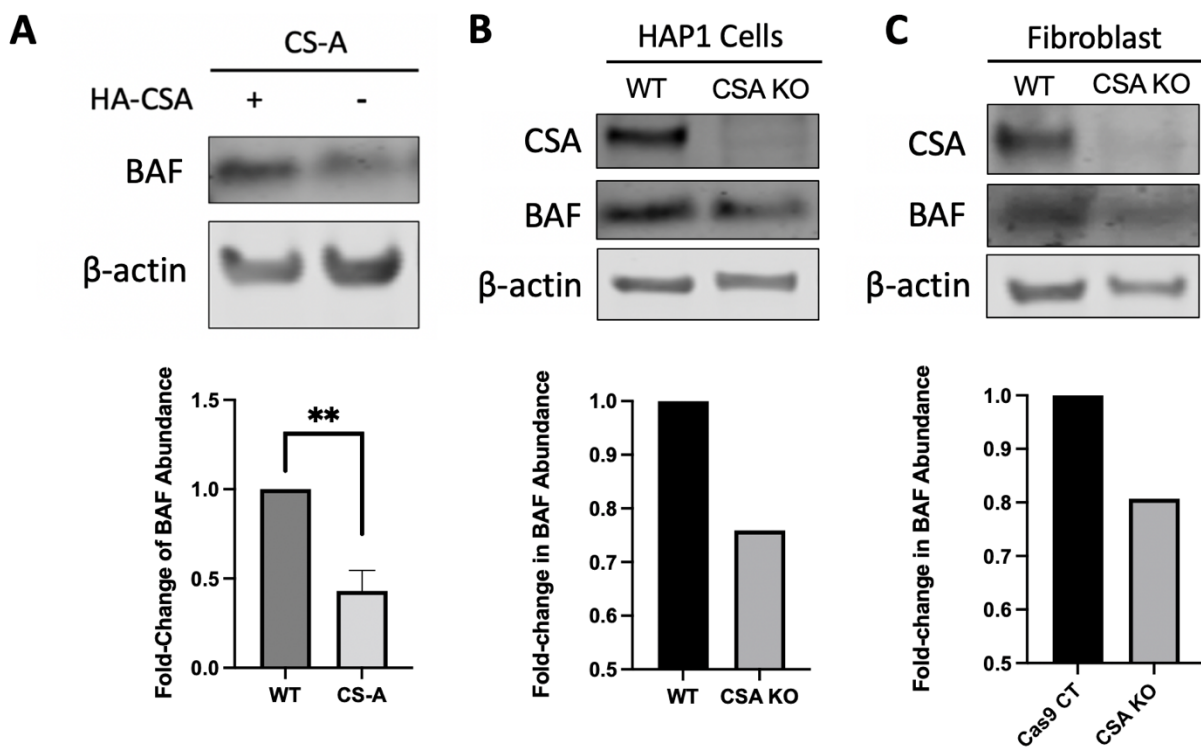


Figure 11. Loss of CSA reduces BAF levels. Representative immunoblots of cell lysates probed for BAF and β -actin as a loading control in (A) CS-A and WT fibroblast (n = 3, **p = 0.0010), (B) HAP-1 WT and CSA knockout (n = 1), and (C) WT and CSA KO fibroblasts (n = 1). Measurements of BAF abundance is normalised to β -actin.

To further investigate how BAF is affected in CS-A cells, we looked at BAF localisation by immunofluorescence. In agreement with our immunoblot results, we found a decreased level of BAF in CS-A cells (**Figure 12A, B**). BAF distributes within the cell in the cytoplasm and

nucleoplasm. A recent report found the cytoplasmic, phosphorylated BAF to play a role in nuclear rupture repair (Halfmann et al., 2019). Accordingly, both the cytoplasmic and nuclear BAF populations, were reduced significantly (**Figure 12C, D**).

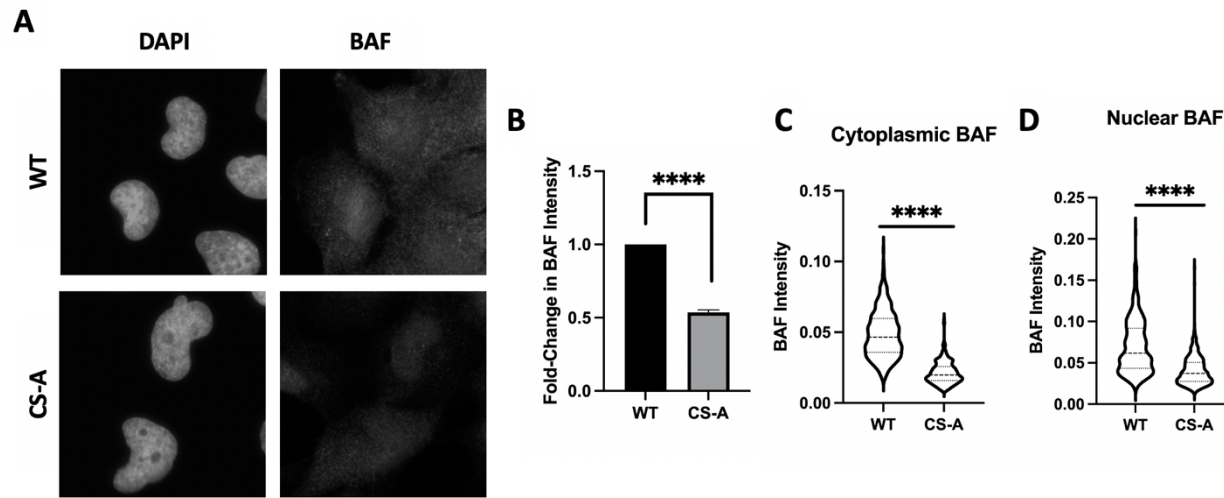


Figure 12. The loss of CSA reduces both nuclear and cytoplasmic levels of BAF. (A) Representative immunofluorescence images of WT and CS-A cells stained for DAPI and BAF. (B) Quantification of the whole-cell average BAF intensity using CellProfiler™. Values of intensity were compiled for WT (n = 422) and CS-A (n= 383) from 3 independent experiments. The two population of data were compared via two-tailed unpaired t test. p-value ****p < 0.0001. Quantification of (C) cytoplasmic and (D) nuclear BAF intensities using CellProfiler™. Values of intensity were compiled for WT (n = 422) and CS-A (n= 383) from 3 independent experiments. The two population of data were compared via two-tailed unpaired t test. p-value ****p < 0.0001.

BAF is reduced in a proteasome-dependent manner in CS-A cells.

The reduction in BAF levels in CS-A cells led us to consider the potential mechanisms by which CSA might regulate BAF levels. Protein levels can be regulated through multiple mechanisms, most notably through protein degradation or increased expression. Proteins can be degraded through the ubiquitin-proteasome system (UPS). Through UPS, a target protein is covalently conjugated to a poly-ubiquitin chain, which can be recognised and degraded by the proteasome. This can be tested through pharmacological inhibition of the proteasome by MG132. In addition to proteasome-dependent protein degradation, protein levels can be regulated at the

translational level, which can be studied by inhibition of translation with the drug cycloheximide (CHX).

To probe for these mechanisms, we analysed the stability of the transiently expressed FLAG-BAF protein in WT and CS-A cells after a time-course treatment with MG132 or CHX. Both WT and CS-A treated with CHX showed the expected and similar reduction in FLAG-BAF level in a time-dependent manner (Figure 13A). Interestingly FLAG-BAF level was significantly stabilised by MG132 in the CS-A cells compared to wild-type cells (Figure 13B). While this experiment requires additional replicates, this result preliminarily suggests that the reduction in BAF levels in CS-A is caused by increased proteasomal degradation.

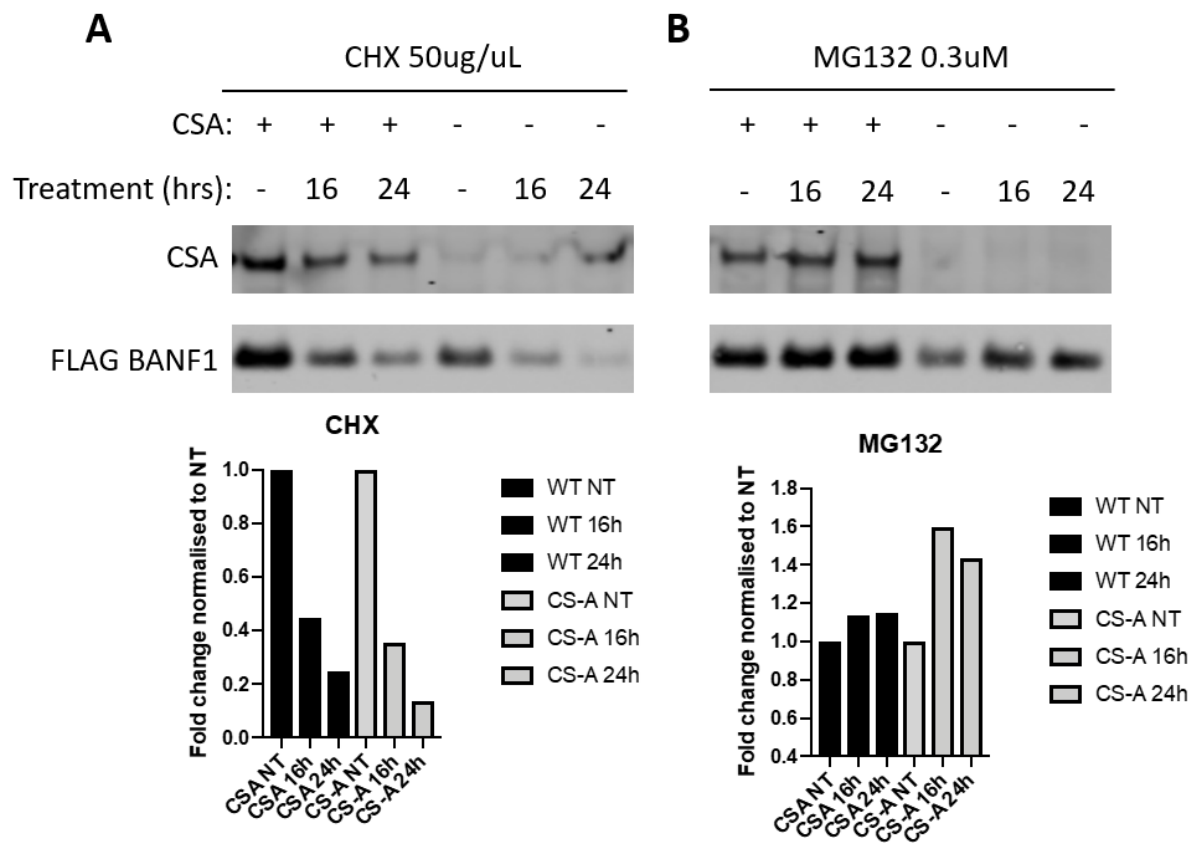


Figure 13. BAF is reduced in a proteasome-dependent manner in CS-A cells. The stability of BAF was analysed by western blotting and normalised to non-treatment groups for the respective cell line. (A-B) CS-A and WT cells were treated with the indicated concentration of Cycloheximide (CHX) (A) or proteasome inhibitor MG132 (B) for 16 or 24 hours.

Overexpression of BAF reduces NE ruptures.

As the level of BAF is lower in the CS-A cells, we hypothesised that restoring its cellular levels may improve the nuclear phenotypes of CS-A cells. By overexpressing FLAG-BAF in both WT and CS-A cells, we found no noticeable increase in nuclear roundness (form factor, **Figure 14A, B**).

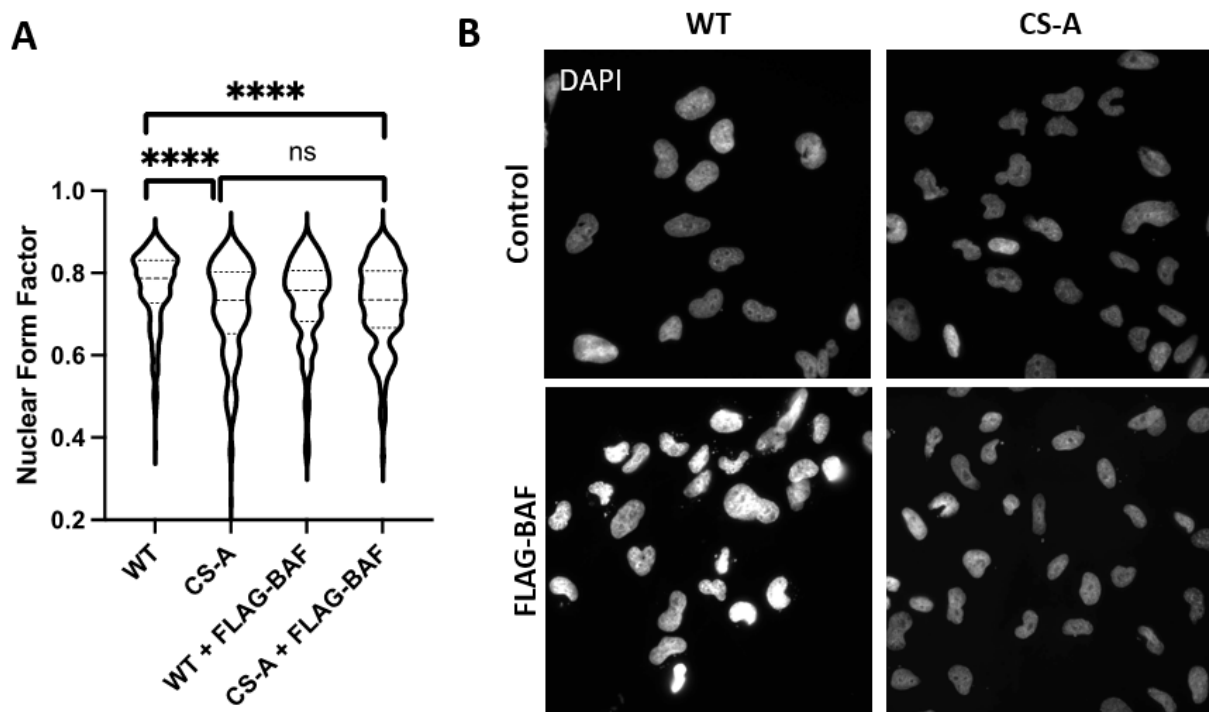


Figure 14. Overexpression of BAF does not significantly affect nuclear shape. (A) Quantification of nuclear form factor using our CellProfiler™ pipeline. Values of form factor were compiled for WT, CS-A, WT + FLAG-BAF, and CS-A + FLAG-BAF ($n = 425, 520, 555, 1155$, respectively) from 3 independent experiments. The two population of data were compared via two-tailed unpaired t test. p-value **** $p < 0.0001$. (B) Representative immunofluorescence images of WT and CS-A, with or without overexpression of FLAG-BAF.

However, we did find that overexpression of FLAG-BAF could reduce the frequency of cGAS perinuclear aggregations as observed by immunofluorescence (**Figure 15A, B**) suggesting a decrease in nuclear envelope ruptures, probably due to improved BAF-mediated nuclear envelope repair or nuclear envelope integrity. Interestingly, WT cells with overexpression of BAF showed increased levels of cGAS aggregations. BAF has been shown to recruit LEM-domain

containing proteins that are involved in the ESCRT-III pathway, which regulate the curvature of membranes and can repair ruptured nuclear membrane. However, an abnormally high level of BAF may result in overactivity of ESCRT-III, resulting in nuclear aberrations that increases ruptures (Vietri et al., 2020a).

Our observation of the elevated cGAS levels in CS-A cells led us to consider whether the overexpression of BAF, in reducing nuclear ruptures, also reduces overall cGAS levels. We found that indeed, overexpression of FLAG-BAF significantly reduced cGAS levels in CS-A cells (Figure 15C). In contrast, WT cells overexpressing FLAG-BAF showed no significant alteration in cGAS abundance.

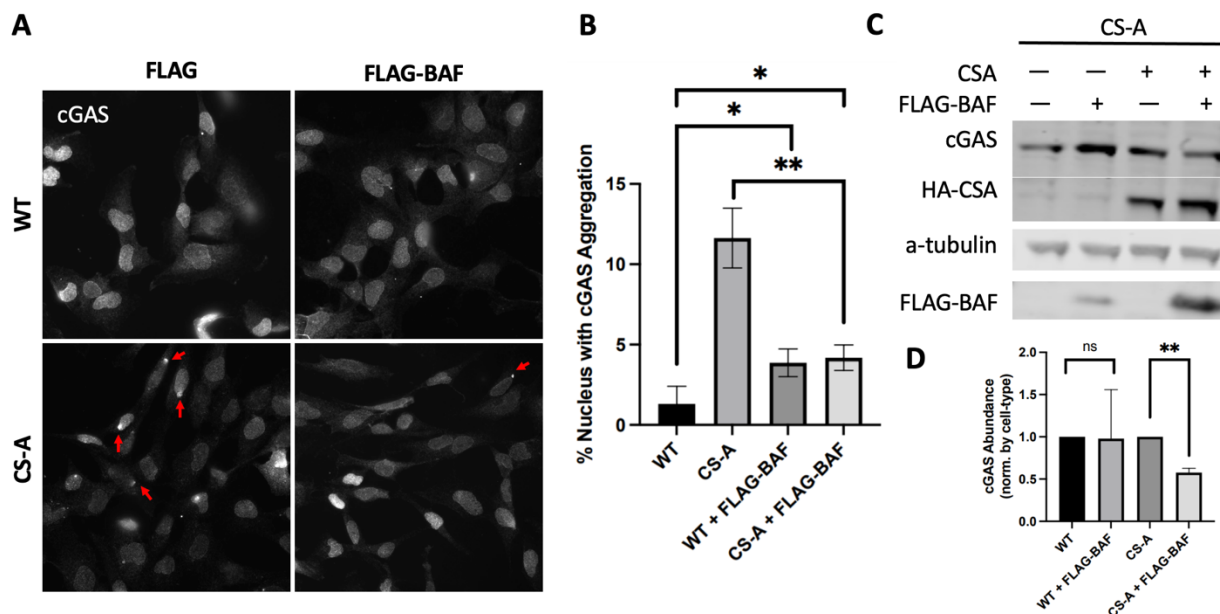


Figure 15. Overexpression of BAF reduces nuclear envelope ruptures. (A) Representative images of cGAS staining for each treatment group. Red arrows point to the cGAS aggregations. (B) Nuclear ruptures were quantified by counting the number of perinuclear cGAS aggregations, and normalising to the number of nuclei. Percentage of nucleus with cGAS aggregation was calculated for WT and CS-A cells, WT cells over-expressing FLAG-BAF (WT + FLAG-BAF), and CS-A cells overexpressing FLAG-BAF (CS-A + FLAG-BAF). Data represents mean \pm S.D. (left to right, n = 425, 520, 555, 1155) from 3 independent experiments. **p = 0.0031, *p = 0.0344. (C) Western blot images of cGAS, HA-CSA, and alpha tubulin as loading control in cells transfected with or without FLAG-BAF. (D) Quantification of western blotting of cGAS from 2 independent experiments, expressed as mean \pm S.D. (n = 2).

The NE function of CSA is independent of its canonical function in DNA damage repair

One of the best-established characteristics of CS-A cell lines is their sensitivity towards DNA damage generated by UV (Laugel, 2013). Due to the role of CSA in TC-NER, its loss in Cockayne Syndrome A hampers the ability of cells to repair UV-induced DNA damage. UV-induced DNA damage can be generated through either exposure to UV light or with pharmacologic agents such as 4-Nitroquinoline 1-oxide (4NQO), which induces DNA damage in a manner similar to UV irradiation.

To assess whether the new role for CSA we identified here in the maintenance of nuclear envelope integrity is related to its known function in DNA damage repair, we set up a 4NQO survival assay in CS-A cells with or without overexpression of BAF. In agreement with previous studies, the loss of CSA resulted in a significant drop of survival after exposure to 4NQO, indicating high sensitivity to this type of damage (Figure 16). Interestingly, this was not affected by the overexpression of FLAG-BAF, as the CS-A cells over-expressing FLAG-BAF were still as sensitive to 4NQO. Therefore, even when the nuclear envelope ruptures are efficiently repaired in CS-A cells through BAF overexpression, the CS-A cells are still as sensitive to DNA damage. Altogether, this suggests that the function of CSA in nuclear envelope integrity maintenance, is independent from its known function in DNA damage repair upon UV-induced damage.

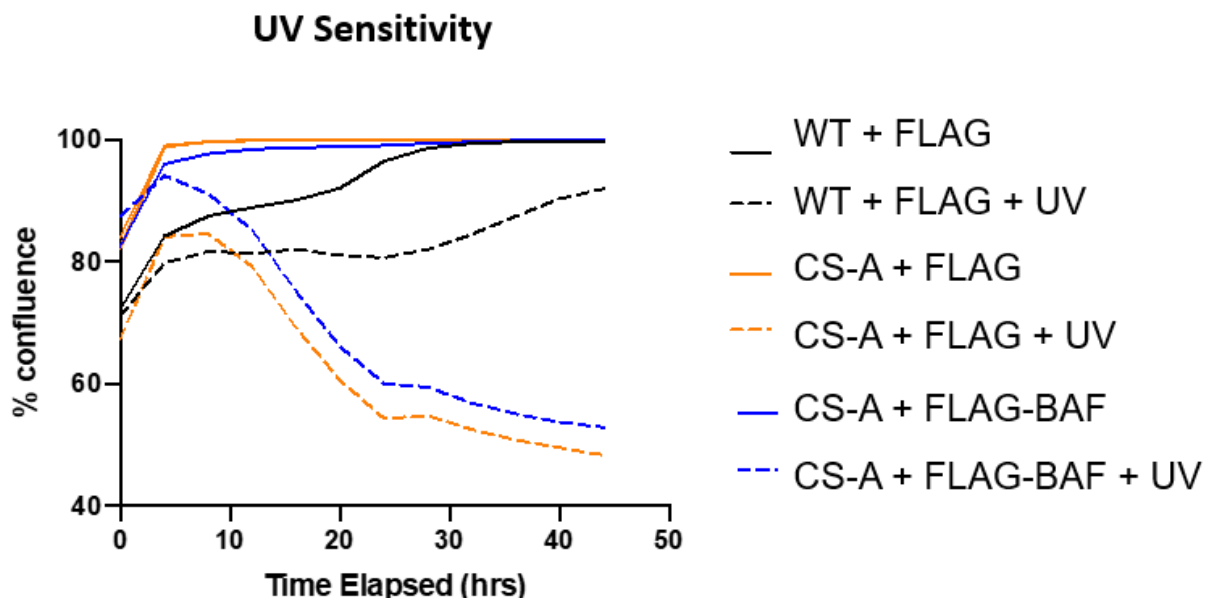


Figure 16. Overexpression of BAF does not rescue UV sensitivity of CS-A cells. WT and CS-A cells were transfected with either FLAG or FLAG-BAF before 1-hour 4NQO treatment, then placed in recovering media and imaged every 4h for 48h. Cell confluence was assessed using an Incucyte microscope and attached software.

CONCLUSION

In this study, we confirmed that the loss of the CSA protein in CS-A patient cells results in greater nuclear deformation, an increased number of nuclear envelope ruptures and nuclear abnormalities. Moreover, we found that as a result of the ruptures, probably because of exposure of the genomic DNA to the cytoplasm, there is an increased activation of the cGAS-STING pathway. Unexpectedly, we found that the loss of CSA results in significantly lower levels of the barrier-to-autointegration factor (BAF), a protein with emerging functions in nuclear envelope rupture repair. We showed that overexpression of BAF rescues the nuclear rupture phenotype in CSA patient cell lines. In studying the mechanistic relationship between CSA and BAF, we found that BAF reduction in CSA patient cells is proteasome-dependent. Finally, this newly identified function for CSA in maintaining nuclear integrity appears to be independent of the known role of CSA in the DNA damage repair.

DISCUSSION

To date, nuclear envelope (NE) defects have not been reported in Cockayne syndrome patient cell lines. While CS is conventionally understood as resulting from defects in UV DNA damage repair, this impairment does not explain all observed phenotypes in patients. Alternative mechanisms such as the maintenance of nuclear envelope integrity may be at play. It is interesting that in the classic HGPS, nuclear envelope ruptures have also been observed (De Vos et al., 2011), suggesting a potential link with ageing that needs further investigation. In addition, the loss of proper organisation of the NE may result in dysregulation of genome organisation and thus in changes in gene expression (Van de Vosse et al., 2011). As the chromatin forms carefully regulated contact points with the NE, such as the lamina-associated domains (LADs) (Briand and Collas, 2020), disruption in these contact points may result in perturbed transcriptional activity. We observed that CS-A nuclei displayed significantly reduced DAPI signal compared to WT. Changes in DAPI intensity may reflect changes in global chromatin compaction that can often result in gene expression changes. Previous studies have used RNA-seq to characterise the change in transcriptome upon UV-induced irradiation of CS-A cells (Epanchintsev et al., 2017). However, a comparison of how stable expression of CSA in CS-A cells restores the transcriptome has yet to be explored. Therefore, it would be interesting to explore the comparative expression profiles of these cells through proteomics or RNA-seq techniques and further characterisation of chromatin

changes using techniques such as ATAC-Seq. In addition, to address whether these chromatin organisation/gene expression changes might be linked to the loss of nuclear envelope integrity in CS-A cells, it would be interesting to investigate the effect of BAF overexpression on these two readouts.

Our data also showed that the loss of CSA in patient-derived cells results in increased activation of the cGAS-STING pathway. Aberrant activation of the cGAS-STING pathway results in inflammation (Zierhut and Funabiki, 2020). Dysregulation in cGAS-STING activation due to mutations underlie autoimmune and inflammatory diseases such as systemic lupus erythematosus (SLE) (Crow and Manel, 2015). Increased inflammation is also known to contribute to ageing and senescence (López-Otín et al., 2013) and phenotypes of premature ageing in CS patients (Carrero et al., 2016). Our findings could therefore provide some clues as to how inflammation may occur in CS patients.

Previous studies reported the interaction between nuclear envelope protein LEMD2 and DDB1 and CUL4A, which form an E3 ligase complex with CSA (Moser et al., 2020). Given this previous report, we hypothesised that CSA might interact with LEMD2 or other NE proteins. Through immunoprecipitation experiments, we observed no interaction between CSA and selected NE proteins. One limitation of our study is that the insolubility of NE proteins can render them difficult to be purified and detected through traditional immunoprecipitation techniques. Alternative methods based on labelling of interaction partners by proximity to a protein of interest, such as biotinylation by antibody-recognition (BAR) (Bar et al., 2018) or APEX-catalysed proximity labelling (Hung et al., 2016), could be used to study the CSA interactome in the future. These experiments will enable us to identify more transient or weak interactors to CSA and provide additional insights into the role of CSA at the nuclear envelope.

While investigating the potential mechanisms underlying the increased nuclear envelope ruptures in CS-A cells, we observed a significant reduction of BAF expression. BAF is known primarily to play a role in post-mitotic NE reformation and cytosolic viral regulation (Halfmann and Roux, 2021). Recent studies have found that cytoplasmic, non-phosphorylated BAF localises to sites of nuclear rupture and recruiting LEM-domain proteins to begin the process of repair (Halfmann et al., 2019). Given the distinction in the roles of repair for the different subcellular populations of BAF, we studied more closely how the loss of CSA impacted the abundance of cytoplasmic and nuclear BAF. Quantification of the intensity of BAF immunofluorescence

demonstrated reduction for both populations. This suggests that the increased susceptibility to nuclear ruptures may result from an overall deficiency of BAF within the cell. To further confirm the change in BAF levels and localisation in CSA patient cells, fractionation experiments will be performed to measure the BAF level in nuclear and cytoplasmic fractions.

The reduction of BAF in CS-A cells suggests a regulatory mechanism linking CSA to BAF. Protein levels can be modulated through transcriptional and translational control or degradation such as by the ubiquitin-proteasome system. We found that the reduction of BAF in CS-A cells appears to be proteasome-dependent. Previous studies have reported BAF to interact with DDB1 and CUL4A. These observations altogether point to a potential model in which the DDB1-CUL4A-CSA E3 ligase complex regulates ubiquitination or neddylation complexes that in turn target BAF for degradation. Thereby the loss of CSA would result in higher levels of these complexes and thus increased BAF degradation. The first step towards testing this model is identifying the complexes involved in BAF degradation. Pharmacological inhibition of conjugating enzymes for ubiquitin or ubiquitin-like proteins can test the role of these modifications in regulating BAF levels. Whether the complexes involved in targeting BAF for proteasomal degradation are more active in CSA patient cells will also need to be confirmed. Alternatively, the changes observed for BAF levels may indirectly result from CSA function at the nuclear envelope. The loss of CSA may result in changes at the NE that indirectly destabilises BAF, leading to reduced BAF abundance. Future work should be aimed at clarifying the validity of these differing paradigms.

While overexpression of BAF significantly reduced nuclear ruptures in CS-A cells, it did not improve the nuclear shape defects. This conflict between the impact of BAF on the nuclear shape and nuclear rupture may be accounted for by two considerations. First, previous studies in other premature ageing syndromes have found that the deformation of the nucleus may be decoupled from other nuclear defects such as blebbing as observed in progeria for example, as one may be rescued by pharmacological agents, while the other remains unchanged (Driscoll et al., 2012). Furthermore, the role of CSA in regulating nuclear shape may be independent of its BAF-dependent role in nuclear envelope rupture repair. We found that overexpression of FLAG-BAF lowered the abundance of cGAS. In investigating further, one interesting avenue would be to explore whether FLAG-BAF overexpression also reduces the phosphorylation of downstream members of the cGAS-STING pathway. Inhibition of this pathway by BAF overexpression may

strengthen the case for BAF as a potential therapeutic target not only for rescuing nuclear ruptures but also for diminishing the downstream immune signalling pathway that directly results in detrimental phenotypes.

Finally, our finding that BAF overexpression does not influence the UV sensitivity of CS-A cells provides a crucial understanding for the link between CSA and BAF within the context of the known functions of CSA. This result suggests that the nuclear envelope function involving CSA and BAF is independent of the well-established role of CSA in UV-induced DNA damage repair.

Together, our findings demonstrate a novel role for CSA in maintaining NE integrity and preventing the activation of inflammatory pathways in patient cells. Further work in elucidating the link between CSA and BAF in the context of nuclear rupture repair may help understand the diversity of phenotypes observed in CS patients.

REFERENCES

- Bakhoum, S.F., Ngo, B., Laughney, A.M., Cavallo, J.-A., Murphy, C.J., Ly, P., Shah, P., Sriram, R.K., Watkins, T.B.K., Taunk, N.K., Duran, M., Pauli, C., Shaw, C., Chadalavada, K., Rajasekhar, V.K., Genovese, G., Venkatesan, S., Birkbak, N.J., McGranahan, N., Lundquist, M., LaPlant, Q., Healey, J.H., Elemento, O., Chung, C.H., Lee, N.Y., Imielinski, M., Nanjangud, G., Pe'er, D., Cleveland, D.W., Powell, S.N., Lammerding, J., Swanton, C., Cantley, L.C., 2018. Chromosomal instability drives metastasis through a cytosolic DNA response. *Nature* 553, 467–472. <https://doi.org/10.1038/nature25432>
- Bar, D.Z., Atkatsh, K., Tavarez, U., Erdos, M.R., Gruenbaum, Y., Collins, F.S., 2018. Biotinylation by antibody recognition—a method for proximity labeling. *Nat Methods* 15, 127–133. <https://doi.org/10.1038/nmeth.4533>
- Bione, S., Maestrini, E., Rivella, S., Mancini, M., Regis, S., Romeo, G., Toniolo, D., 1994. Identification of a novel X-linked gene responsible for Emery-Dreifuss muscular dystrophy. *Nat Genet* 8, 323–327. <https://doi.org/10.1038/ng1294-323>
- Bonne, G., Di Barletta, M.R., Varnous, S., Bécane, H.M., Hammouda, E.H., Merlini, L., Muntoni, F., Greenberg, C.R., Gary, F., Urtizberea, J.A., Duboc, D., Fardeau, M., Toniolo, D., Schwartz, K., 1999. Mutations in the gene encoding lamin A/C cause autosomal dominant Emery-Dreifuss muscular dystrophy. *Nat Genet* 21, 285–288. <https://doi.org/10.1038/6799>
- Briand, N., Collas, P., 2020. Lamina-associated domains: peripheral matters and internal affairs. *Genome Biology* 21, 85. <https://doi.org/10.1186/s13059-020-02003-5>
- Britton, S., Coates, J., Jackson, S.P., 2013. A new method for high-resolution imaging of Ku foci to decipher mechanisms of DNA double-strand break repair. *Journal of Cell Biology* 202, 579–595. <https://doi.org/10.1083/jcb.201303073>
- Carrero, D., Soria-Valles, C., López-Otín, C., 2016. Hallmarks of progeroid syndromes: lessons from mice and reprogrammed cells. *Disease Models & Mechanisms* 9, 719–735. <https://doi.org/10.1242/dmm.024711>
- Charras, G.T., Coughlin, M., Mitchison, T.J., Mahadevan, L., 2008. Life and Times of a Cellular Bleb. *Biophysical Journal* 94, 1836–1853. <https://doi.org/10.1529/biophysj.107.113605>
- Chu, F.-Y., Haley, S.C., Zidovska, A., 2017. On the origin of shape fluctuations of the cell nucleus. *PNAS* 114, 10338–10343. <https://doi.org/10.1073/pnas.1702226114>
- Cimini, D., Cameron, L.A., Salmon, E.D., 2004. Anaphase spindle mechanics prevent mis-segregation of merotelically oriented chromosomes. *Curr Biol* 14, 2149–2155. <https://doi.org/10.1016/j.cub.2004.11.029>
- Citterio, E., Van Den Boom, V., Schnitzler, G., Kanaar, R., Bonte, E., Kingston, R.E., Hoeijmakers, J.H., Vermeulen, W., 2000. ATP-dependent chromatin remodeling by the Cockayne syndrome B DNA repair-transcription-coupling factor. *Mol Cell Biol* 20, 7643–7653. <https://doi.org/10.1128/MCB.20.20.7643-7653.2000>
- Cockayne, E.A., 1936. Dwarfism with retinal atrophy and deafness. *Arch Dis Child* 11, 1–8.
- Cramer, L.P., Mitchison, T.J., 1995. Myosin is involved in postmitotic cell spreading. *Journal of Cell Biology* 131, 179–189. <https://doi.org/10.1083/jcb.131.1.179>
- Crow, Y.J., Manel, N., 2015. Aicardi–Goutières syndrome and the type I interferonopathies. *Nat Rev Immunol* 15, 429–440. <https://doi.org/10.1038/nri3850>

- De Vos, W.H., Houben, F., Kamps, M., Malhas, A., Verheyen, F., Cox, J., Manders, E.M.M., Verstraeten, V.L.R.M., van Steensel, M.A.M., Marcelis, C.L.M., van den Wijngaard, A., Vaux, D.J., Ramaekers, F.C.S., Broers, J.L.V., 2011. Repetitive disruptions of the nuclear envelope invoke temporary loss of cellular compartmentalization in laminopathies. *Human Molecular Genetics* 20, 4175–4186. <https://doi.org/10.1093/hmg/ddr344>
- Denais, C.M., Gilbert, R.M., Isermann, P., McGregor, A.L., Lindert, M. te, Weigelin, B., Davidson, P.M., Friedl, P., Wolf, K., Lammerding, J., 2016. Nuclear envelope rupture and repair during cancer cell migration. *Science* 352, 353–358. <https://doi.org/10.1126/science.aad7297>
- Doherty, F.J., Dawson, S., Mayer, R.J., 2002. The ubiquitin-proteasome pathway of intracellular proteolysis. *Essays Biochem* 38, 51–63. <https://doi.org/10.1042/bse0380051>
- Driscoll, M.K., Albanese, J.L., Xiong, Z.-M., Mailman, M., Losert, W., Cao, K., 2012. Automated image analysis of nuclear shape: what can we learn from a prematurely aged cell? *Aging (Albany NY)* 4, 119–132. <https://doi.org/10.18632/aging.100434>
- Earle, A.J., Kirby, T.J., Fedorchak, G.R., Isermann, P., Patel, J., Iravanti, S., Moore, S.A., Bonne, G., Wallrath, L.L., Lammerding, J., 2020. Mutant lamins cause nuclear envelope rupture and DNA damage in skeletal muscle cells. *Nat. Mater.* 19, 464–473. <https://doi.org/10.1038/s41563-019-0563-5>
- Epanchintsev, A., Costanzo, F., Rauschendorf, M.-A., Caputo, M., Ye, T., Donnio, L.-M., Proietti-de-Santis, L., Coin, F., Laugel, V., Egly, J.-M., 2017. Cockayne's Syndrome A and B Proteins Regulate Transcription Arrest after Genotoxic Stress by Promoting ATF3 Degradation. *Mol Cell* 68, 1054–1066.e6. <https://doi.org/10.1016/j.molcel.2017.11.009>
- Evans, H.J., Neary, G.J., Williamson, F.S., 1959. The Relative Biological Efficiency of Single Doses of Fast Neutrons and Gamma-rays on Vicia Faba Roots and the Effect of Oxygen. *International Journal of Radiation Biology and Related Studies in Physics, Chemistry and Medicine* 1, 216–229. <https://doi.org/10.1080/09553005914550311>
- Fousteri, M., Mullenders, L.H., 2008. Transcription-coupled nucleotide excision repair in mammalian cells: molecular mechanisms and biological effects. *Cell Res* 18, 73–84. <https://doi.org/10.1038/cr.2008.6>
- Fousteri, M., Vermeulen, W., van Zeeland, A.A., Mullenders, L.H.F., 2006. Cockayne syndrome A and B proteins differentially regulate recruitment of chromatin remodeling and repair factors to stalled RNA polymerase II in vivo. *Mol Cell* 23, 471–482. <https://doi.org/10.1016/j.molcel.2006.06.029>
- Funkhouser, C.M., Sknepnek, R., Shimi, T., Goldman, A.E., Goldman, R.D., Cruz, M.O. de la, 2013. Mechanical model of blebbing in nuclear lamin meshworks. *PNAS* 110, 3248–3253. <https://doi.org/10.1073/pnas.1300215110>
- Goldman, R.D., Shumaker, D.K., Erdos, M.R., Eriksson, M., Goldman, A.E., Gordon, L.B., Gruenbaum, Y., Khuon, S., Mendez, M., Varga, R., Collins, F.S., 2004. Accumulation of mutant lamin A causes progressive changes in nuclear architecture in Hutchinson–Gilford progeria syndrome. *PNAS* 101, 8963–8968. <https://doi.org/10.1073/pnas.0402943101>
- Groisman, R., Polanowska, J., Kuraoka, I., Sawada, J., Saijo, M., Drapkin, R., Kisseelev, A.F., Tanaka, K., Nakatani, Y., 2003. The ubiquitin ligase activity in the DDB2 and CSA

- complexes is differentially regulated by the COP9 signalosome in response to DNA damage. *Cell* 113, 357–367. [https://doi.org/10.1016/s0092-8674\(03\)00316-7](https://doi.org/10.1016/s0092-8674(03)00316-7)
- Gu, M., LaJoie, D., Chen, O.S., Appen, A. von, Ladinsky, M.S., Redd, M.J., Nikolova, L., Bjorkman, P.J., Sundquist, W.I., Ullman, K.S., Frost, A., 2017. LEM2 recruits CHMP7 for ESCRT-mediated nuclear envelope closure in fission yeast and human cells. *PNAS* 114, E2166–E2175. <https://doi.org/10.1073/pnas.1613916114>
- Güttinger, S., Laurell, E., Kutay, U., 2009. Orchestrating nuclear envelope disassembly and reassembly during mitosis. *Nat Rev Mol Cell Biol* 10, 178–191. <https://doi.org/10.1038/nrm2641>
- Halfmann, C.T., Roux, K.J., 2021. Barrier-to-autointegration factor: a first responder for repair of nuclear ruptures. *Cell Cycle* 20, 647–660. <https://doi.org/10.1080/15384101.2021.1892320>
- Halfmann, C.T., Sears, R.M., Katiyar, A., Busselman, B.W., Aman, L.K., Zhang, Q., O'Bryan, C.S., Angelini, T.E., Lele, T.P., Roux, K.J., 2019. Repair of nuclear ruptures requires barrier-to-autointegration factor. *J Cell Biol* 218, 2136–2149. <https://doi.org/10.1083/jcb.201901116>
- Hanahan, D., Weinberg, R.A., 2011. Hallmarks of cancer: the next generation. *Cell* 144, 646–674. <https://doi.org/10.1016/j.cell.2011.02.013>
- Hetzer, M.W., 2010. The Nuclear Envelope. *Cold Spring Harb Perspect Biol* 2, a000539. <https://doi.org/10.1101/cshperspect.a000539>
- Hung, V., Udeshi, N.D., Lam, S.S., Loh, K.H., Cox, K.J., Pedram, K., Carr, S.A., Ting, A.Y., 2016. Spatially resolved proteomic mapping in living cells with the engineered peroxidase APEX2. *Nat Protoc* 11, 456–475. <https://doi.org/10.1038/nprot.2016.018>
- Jamin, A., Wiebe, M.S., 2015. Barrier to Autointegration Factor (BANF1): interwoven roles in nuclear structure, genome integrity, innate immunity, stress responses and progeria. *Curr Opin Cell Biol* 34, 61–68. <https://doi.org/10.1016/j.ceb.2015.05.006>
- Jin, J., Arias, E.E., Chen, J., Harper, J.W., Walter, J.C., 2006. A family of diverse Cul4-Ddb1-interacting proteins includes Cdt2, which is required for S phase destruction of the replication factor Cdt1. *Mol Cell* 23, 709–721. <https://doi.org/10.1016/j.molcel.2006.08.010>
- Kennedy, R.M., Rowe, V.D., Kepes, J.J., 1980. Cockayne syndrome: an atypical case. *Neurology* 30, 1268–1272. <https://doi.org/10.1212/wnl.30.12.1268>
- Kwon, M., Leibowitz, M.L., Lee, J.-H., 2020. Small but mighty: the causes and consequences of micronucleus rupture. *Exp Mol Med* 52, 1777–1786. <https://doi.org/10.1038/s12276-020-00529-z>
- Lake, R.J., Fan, H.-Y., 2013. Structure, function and regulation of CSB: a multi-talented gymnast. *Mech Ageing Dev* 134, 202–211. <https://doi.org/10.1016/j.mad.2013.02.004>
- Laugel, V., 2013. Cockayne syndrome: The expanding clinical and mutational spectrum. *Mechanisms of Ageing and Development, Special Issue on the segmental progeria Cockayne syndrome* 134, 161–170. <https://doi.org/10.1016/j.mad.2013.02.006>
- Laugel, V., Dalloz, C., Durand, M., Sauvanaud, F., Kristensen, U., Vincent, M.C., Pasquier, L., Odent, S., Cormier-Daire, V., Gener, B., Tobias, E.S., Tolmie, J.L., Martin-Coignard, D., Drouin-Garraud, V., Heron, D., Journel, H., Raffo, E., Vigneron, J., Lyonnet, S., Murday, V., Gubser-Mercati, D., Funalot, B., Brueton, L., Pozo, J.S. del, Muñoz, E., Gennery, A.R.,

- Salih, M., Noruzinia, M., Prescott, K., Ramos, L., Stark, Z., Fieggen, K., Chabrol, B., Sarda, P., Edery, P., Bloch-Zupan, A., Fawcett, H., Pham, D., Egly, J.M., Lehmann, A.R., Sarasin, A., Dollfus, H., 2010. Mutation update for the CSB/ERCC6 and CSA/ERCC8 genes involved in Cockayne syndrome. *Human Mutation* 31, 113–126.
<https://doi.org/10.1002/humu.21154>
- Le Berre, M., Aubertin, J., Piel, M., 2012. Fine control of nuclear confinement identifies a threshold deformation leading to lamina rupture and induction of specific genes. *Integr Biol (Camb)* 4, 1406–1414. <https://doi.org/10.1039/c2ib20056b>
- Lee, Y.L., Burke, B., 2018. LINC complexes and nuclear positioning. *Semin Cell Dev Biol* 82, 67–76. <https://doi.org/10.1016/j.semcdcb.2017.11.008>
- Lionetti, M.C., Bonfanti, S., Fumagalli, M.R., Budrikis, Z., Font-Clos, F., Costantini, G., Chepizhko, O., Zapperi, S., La Porta, C.A.M., 2020. Chromatin and Cytoskeletal Tethering Determine Nuclear Morphology in Progerin-Expressing Cells. *Biophysical Journal* 118, 2319–2332. <https://doi.org/10.1016/j.bpj.2020.04.001>
- Ljungman, M., Zhang, F., 1996. Blockage of RNA polymerase as a possible trigger for u.v. light-induced apoptosis. *Oncogene* 13, 823–831.
- López-Otín, C., Blasco, M.A., Partridge, L., Serrano, M., Kroemer, G., 2013. The Hallmarks of Aging. *Cell* 153, 1194–1217. <https://doi.org/10.1016/j.cell.2013.05.039>
- Lowry, R.B., 1982. Early onset of Cockayne syndrome. *Am J Med Genet* 13, 209–210.
<https://doi.org/10.1002/ajmg.1320130211>
- Maciejowski, J., Hatch, E.M., 2020. Nuclear Membrane Rupture and Its Consequences. *Annu Rev Cell Dev Biol* 36, 85–114. <https://doi.org/10.1146/annurev-cellbio-020520-120627>
- Mackenzie, K.J., Carroll, P., Martin, C.-A., Murina, O., Fluteau, A., Simpson, D.J., Olova, N., Sutcliffe, H., Rainger, J.K., Leitch, A., Osborn, R.T., Wheeler, A.P., Nowotny, M., Gilbert, N., Chandra, T., Reijns, M.A.M., Jackson, A.P., 2017. cGAS surveillance of micronuclei links genome instability to innate immunity. *Nature* 548, 461–465.
<https://doi.org/10.1038/nature23449>
- Marteijn, J.A., Lans, H., Vermeulen, W., Hoeijmakers, J.H.J., 2014. Understanding nucleotide excision repair and its roles in cancer and ageing. *Nat Rev Mol Cell Biol* 15, 465–481. <https://doi.org/10.1038/nrm3822>
- Moser, B., Basílio, J., Gotzmann, J., Brachner, A., Foisner, R., 2020. Comparative Interactome Analysis of Emerin, MAN1 and LEM2 Reveals a Unique Role for LEM2 in Nucleotide Excision Repair. *Cells* 9, 463. <https://doi.org/10.3390/cells9020463>
- Moyer, D.B., Marquis, P., Shertzer, M.E., Burton, B.K., 1982. Cockayne syndrome with early onset of manifestations. *Am J Med Genet* 13, 225–230.
<https://doi.org/10.1002/ajmg.1320130213>
- Muchir, A., Medioni, J., Laluc, M., Massart, C., Arimura, T., van der Kooi, A.J., Desguerre, I., Mayer, M., Ferrer, X., Briault, S., Hirano, M., Worman, H.J., Mallet, A., Wehnert, M., Schwartz, K., Bonne, G., 2004. Nuclear envelope alterations in fibroblasts from patients with muscular dystrophy, cardiomyopathy, and partial lipodystrophy carrying lamin A/C gene mutations. *Muscle Nerve* 30, 444–450. <https://doi.org/10.1002/mus.20122>
- Nardo, T., Oneda, R., Spivak, G., Vaz, B., Mortier, L., Thomas, P., Orioli, D., Laugel, V., Stary, A., Hanawalt, P.C., Sarasin, A., Stefanini, M., 2009. A UV-sensitive syndrome patient with a

- specific CSA mutation reveals separable roles for CSA in response to UV and oxidative DNA damage. PNAS 106, 6209–6214. <https://doi.org/10.1073/pnas.0902113106>
- Olmos, Y., Perdrix-Rosell, A., Carlton, J.G., 2016. Membrane Binding by CHMP7 Coordinates ESCRT-III-Dependent Nuclear Envelope Reformation. Curr Biol 26, 2635–2641. <https://doi.org/10.1016/j.cub.2016.07.039>
- Penfield, L., Wysolmerski, B., Mauro, M., Farhadifar, R., Martinez, M.A., Biggs, R., Wu, H.-Y., Broberg, C., Needleman, D., Bahmanyar, S., 2018. Dynein pulling forces counteract lamin-mediated nuclear stability during nuclear envelope repair. MBoC 29, 852–868. <https://doi.org/10.1091/mbc.E17-06-0374>
- Raab, M., Gentili, M., Belly, H. de, Thiam, H.-R., Vargas, P., Jimenez, A.J., Lautenschlaeger, F., Voituriez, R., Lennon-Duménil, A.-M., Manel, N., Piel, M., 2016. ESCRT III repairs nuclear envelope ruptures during cell migration to limit DNA damage and cell death. Science 352, 359–362. <https://doi.org/10.1126/science.aad7611>
- Rapin, I., Weidenheim, K., Lindenbaum, Y., Rosenbaum, P., Merchant, S.N., Krishna, S., Dickson, D.W., 2006. Cockayne syndrome in adults: review with clinical and pathologic study of a new case. J Child Neurol 21, 991–1006. <https://doi.org/10.1177/08830738060210110101>
- Rieckher, M., Garinis, G.A., Schumacher, B., 2021. Molecular pathology of rare progeroid diseases. Trends in Molecular Medicine. <https://doi.org/10.1016/j.molmed.2021.06.011>
- Saijo, M., 2013. The role of Cockayne syndrome group A (CSA) protein in transcription-coupled nucleotide excision repair. Mechanisms of Ageing and Development, Special Issue on the segmental progeria Cockayne syndrome 134, 196–201. <https://doi.org/10.1016/j.mad.2013.03.008>
- Samwer, M., Schneider, M.W.G., Hoefler, R., Schmalhorst, P.S., Jude, J.G., Zuber, J., Gerlich, D.W., 2017. DNA Cross-Bridging Shapes a Single Nucleus from a Set of Mitotic Chromosomes. Cell 170, 956–972.e23. <https://doi.org/10.1016/j.cell.2017.07.038>
- Sarker, A.H., Tsutakawa, S.E., Kostek, S., Ng, C., Shin, D.S., Peris, M., Campeau, E., Tainer, J.A., Nogales, E., Cooper, P.K., 2005. Recognition of RNA Polymerase II and Transcription Bubbles by XPG, CSB, and TFIH: Insights for Transcription-Coupled Repair and Cockayne Syndrome. Molecular Cell 20, 187–198. <https://doi.org/10.1016/j.molcel.2005.09.022>
- Shah, P., Wolf, K., Lammerding, J., 2017. Bursting the Bubble – Nuclear Envelope Rupture as a Path to Genomic Instability? Trends in Cell Biology 27, 546–555. <https://doi.org/10.1016/j.tcb.2017.02.008>
- Srivastava, N., Nader, G.P. de F., Williart, A., Rollin, R., Cuvelier, D., Lomakin, A., Piel, M., 2021. Nuclear fragility, blaming the blebs. Current Opinion in Cell Biology, Cell Nucleus 70, 100–108. <https://doi.org/10.1016/j.ceb.2021.01.007>
- Stankevicius, L.D.C., Urbanska, M., Flormann, D.A., Terriac, E., Mostajeran, Z., Gad, A.K.B., Cheng, F., Eriksson, J.E., Lautenschläger, F., 2019. Vimentin provides the mechanical resilience required for amoeboid migration and protection of the nucleus. <https://doi.org/10.1101/720946>
- Stephens, A.D., Banigan, E.J., Marko, J.F., 2017. Separate roles for chromatin and lamins in nuclear mechanics. Nucleus 9, 119–124. <https://doi.org/10.1080/19491034.2017.1414118>

- Stich, H.F., Rosin, M.P., 1984. Micronuclei in exfoliated human cells as a tool for studies in cancer risk and cancer intervention. *Cancer Lett* 22, 241–253.
[https://doi.org/10.1016/0304-3835\(84\)90159-9](https://doi.org/10.1016/0304-3835(84)90159-9)
- Svejstrup, J.Q., 2002. Mechanisms of transcription-coupled DNA repair. *Nat Rev Mol Cell Biol* 3, 21–29. <https://doi.org/10.1038/nrm703>
- Tantin, D., Kansal, A., Carey, M., 1997. Recruitment of the putative transcription-repair coupling factor CSB/ERCC6 to RNA polymerase II elongation complexes. *Mol Cell Biol* 17, 6803–6814. <https://doi.org/10.1128/MCB.17.12.6803>
- Thompson, S.L., Compton, D.A., 2011. Chromosome missegregation in human cells arises through specific types of kinetochore–microtubule attachment errors. *PNAS* 108, 17974–17978. <https://doi.org/10.1073/pnas.1109720108>
- Troelstra, C., van Gool, A., de Wit, J., Vermeulen, W., Bootsma, D., Hoeijmakers, J.H., 1992. ERCC6, a member of a subfamily of putative helicases, is involved in Cockayne's syndrome and preferential repair of active genes. *Cell* 71, 939–953.
[https://doi.org/10.1016/0092-8674\(92\)90390-x](https://doi.org/10.1016/0092-8674(92)90390-x)
- Ungrich, R., Kutay, U., 2017. Mechanisms and functions of nuclear envelope remodelling. *Nat Rev Mol Cell Biol* 18, 229–245. <https://doi.org/10.1038/nrm.2016.153>
- Van de Vosse, D.W., Wan, Y., Wozniak, R.W., Aitchison, J.D., 2011. Role of the nuclear envelope in genome organization and gene expression. *Wiley Interdiscip Rev Syst Biol Med* 3, 147–166. <https://doi.org/10.1002/wsbm.101>
- van den Boom, V., Citterio, E., Hoogstraten, D., Zotter, A., Egly, J.-M., van Cappellen, W.A., Hoeijmakers, J.H.J., Houtsmuller, A.B., Vermeulen, W., 2004. DNA damage stabilizes interaction of CSB with the transcription elongation machinery. *J Cell Biol* 166, 27–36.
<https://doi.org/10.1083/jcb.200401056>
- Venturini, V., Pezzano, F., Castro, F.C., Häkkinen, H.-M., Jiménez-Delgado, S., Colomer-Rosell, M., Marro, M., Tolosa-Ramon, Q., Paz-López, S., Valverde, M.A., Weghuber, J., Loza-Alvarez, P., Krieg, M., Wieser, S., Ruprecht, V., 2020. The nucleus measures shape changes for cellular proprioception to control dynamic cell behavior. *Science* 370.
<https://doi.org/10.1126/science.aba2644>
- Vietri, M., Radulovic, M., Stenmark, H., 2020a. The many functions of ESCRTs. *Nat Rev Mol Cell Biol* 21, 25–42. <https://doi.org/10.1038/s41580-019-0177-4>
- Vietri, M., Schultz, S.W., Bellanger, A., Jones, C.M., Petersen, L.I., Raiborg, C., Skarpen, E., Pedurupillay, C.R.J., Kjos, I., Kip, E., Timmer, R., Jain, A., Collas, P., Knorr, R.L., Grellscheid, S.N., Kusumaatmaja, H., Brech, A., Micci, F., Stenmark, H., Campsteijn, C., 2020b. Unrestrained ESCRT-III drives micronuclear catastrophe and chromosome fragmentation. *Nat Cell Biol* 22, 856–867. <https://doi.org/10.1038/s41556-020-0537-5>
- von Appen, A., LaJoie, D., Johnson, I.E., Trnka, M.J., Pick, S.M., Burlingame, A.L., Ullman, K.S., Frost, A., 2020. LEM2 phase separation promotes ESCRT-mediated nuclear envelope reformation. *Nature* 582, 115–118. <https://doi.org/10.1038/s41586-020-2232-x>
- Webster, B.M., Thaller, D.J., Jäger, J., Ochmann, S.E., Borah, S., Lusk, C.P., 2016. Chm7 and Heh1 collaborate to link nuclear pore complex quality control with nuclear envelope sealing. *EMBO J* 35, 2447–2467. <https://doi.org/10.15252/embj.201694574>
- Wilson, B.T., Stark, Z., Sutton, R.E., Danda, S., Ekbote, A.V., Elsayed, S.M., Gibson, L., Goodship, J.A., Jackson, A.P., Keng, W.T., King, M.D., McCann, E., Motojima, T., Murray, J.E.,

- Omata, T., Pilz, D., Pope, K., Sugita, K., White, S.M., Wilson, I.J., 2016. The Cockayne Syndrome Natural History (CoSyNH) study: clinical findings in 102 individuals and recommendations for care. *Genet Med* 18, 483–493.
<https://doi.org/10.1038/gim.2015.110>
- Wong, X., Stewart, C.L., 2020. The Laminopathies and the Insights They Provide into the Structural and Functional Organization of the Nucleus. *Annual Review of Genomics and Human Genetics* 21, 263–288. <https://doi.org/10.1146/annurev-genom-121219-083616>
- Ye, C.J., Sharpe, Z., Alemara, S., Mackenzie, S., Liu, G., Abdallah, B., Horne, S., Regan, S., Heng, H.H., 2019. Micronuclei and Genome Chaos: Changing the System Inheritance. *Genes (Basel)* 10, E366. <https://doi.org/10.3390/genes10050366>
- Zierhut, C., Funabiki, H., 2020. Regulation and Consequences of cGAS Activation by Self-DNA. *Trends in Cell Biology* 30, 594–605. <https://doi.org/10.1016/j.tcb.2020.05.006>